Material characterisation of existing masonryfor URM abacus

Jafari, Samira; Esposito, Rita

Publication date
2018

Document Version
Final published version

Citation (APA)
Jafari, S., & Esposito, R. (2018). *Material characterisation of existing masonryfor URM abacus*. Delft University of Technology.

Project number	C31B67
File reference	C31B67WP1-14
Date	February 18, 2018
Corresponding author	Samira Jafari (s.jafari@tudelft.nl)

TU Delft Large-Scale Testing Campaign 2016

MATERIAL CHARACTERISATION OF EXISTING MASONRY FOR URM ABACUS

Authors: Samira Jafari, Rita Esposito
Collaborators: Jakub Pawlowicz

***Cite as**: Jafari, S., Esposito,* Material characterisation of existing masonry for URM abacus*. Report No. C31B67WP1-14, 18 February 2018. Delft University of Technology.*

This document is made available via the website 'Structural Response to Earthquakes' and the TU Delft repository. While citing, please verify if there are recent updates of this research in the form of scientific papers.

This research work was funded by NAM Structural Upgrading stream.

Table of Contents

1 Introduction

Investigation of the material properties of different types of existing masonry in the Groningen area was carried out in the current and past projects aiming to establish an abacus for Dutch masonry. The compilation of the database is essential to undertake buildings' assessment, because it allows determining the input material parameters for practitioners. The considered masonry objects were built in the period between 1920 and 2013 and were mainly made of clay brick masonry and calcium silicate (CS) brick masonry. Compression, tension and shear tests were conducted to characterise the mechanical properties of masonry specimens ([1-2], Table 1).

With the scope of enriching the URM abacus properties established from the experimental campaigns of 2014 and 2015, a plan of approach (PoA) for further tests was developed by TU Delft within the "NAM Structural Upgrading Project" in 2016/2017 [3]. In order to provide more data for certain construction periods, clay brick masonry houses built before 1920 and calcium silicate (CS) brick masonry houses built after 1985 were identified as testing objects of this campaign. The aim is to provide a complete characterisation of each object whenever possible.

In this report, the experimental results carried out on samples extracted from existing masonry building in the testing campaign 2016/2017 are reported. Section 3 gives an overview of the houses where sampling took place. Test results on the compressive and flexural strength of masonry unit (brick) are given in Section 4 and Section 5, respectively. The density of masonry samples is reported in Section 6. Test results on the compression, bending and shear properties are reported from Section 7 to Section 10. Eventually, a summary of the material properties is reported in Section 11.

Table 1 – Destructive material tests for the characterisation of masonry.

	Type of test			**Material property**
Masonry units	Compression			Compressive strength Stress-strain relationship in compression
	Bending			Flexural strength of brick Elastic modulus Stress-strain relationship in bending
Masonry	Compression	Vertical		Compressive strength Young's modulus Fracture energy in compression Poisson ratio Stress-strain relationship in compression (pre- and post-peak)
		Horizontal		
	Bending	Out-of-plane	Vertical	Flexural strength with plane of failure parallel to bed joints Stress-strain relationship Fracture energy in bending
			Horizontal	Flexural strength with plane of failure perpendicular to bed joints Stress-strain relationship Fracture energy in bending
		In-plane	Vertical	Flexural strength with the moment vector perpendicular to the plane of the wall Stress-strain relationship Fracture energy in bending
	Shear test			Initial and residual shear strength Initial and residual shear friction coefficient Mode-II fracture energy Shear stress vs. shear displacement relationship (pre- and post-peak)
	Bond wrench			Flexural bond strength

2 Nomenclature

2.1 Symbols

This report adopts mainly the nomenclature used in Eurocode 6 [4]. In addition, symbols used in the codes for testing are adopted.

α	Masonry (bed joint) angle of internal friction
α_{res}	Masonry (bed joint) residual angle of internal friction
ν	Poisson ratio of masonry
μ	Masonry (bed joint) shear strength coefficient
μ_{res}	Masonry (bed joint) residual shear strength coefficient
ε_p	Strain associated with peak strength in vertical compression test
$\varepsilon_{p,h}$	Strain associated with peak strength in horizontal compression test
d_1	Distance between bearing supports
d_2	Distance between loading supports
d_3	Distance between the loading and bearing supports (four-point bending test)
f_b	Normalised compressive strength of masonry unit
f_b^*	Compressive strength of masonry unit
f_{bt}	Flexural strength of masonry unit
$f_m^{'}$	Compressive strength of masonry in the direction perpendicular to the bed joints
$f_{m,h}^{'}$	Compressive strength of masonry in the direction parallel to the bed joints
f_p	Applied lateral pre-compression stress
f_{x1}	Masonry flexural strength with the moment vector parallel to the bed joints and in the plane of the wall, which generates a plane of failure parallel to the bed joints
f_{x2}	Masonry flexural strength with the moment vector orthogonal to the bed joints and in the plane of the wall, which generates a plane of failure perpendicular to the bed joints
f_{x3}	Masonry flexural strength with the moment vector orthogonal to the plane of the wall
f_{v0}	Masonry (bed joint) initial shear strength
$f_{v0,res}$	Masonry (bed joint) residual initial shear strength
f_w	Masonry uniaxial bond strength between the masonry unit and the mortar
l_s	Length of the masonry specimen as built
l_u	Length of the masonry unit as used in the construction of masonry
h_s	Height of the masonry specimen as built
h_u	Height of the masonry unit as used in the construction
t_s	Thickness of the masonry specimen as built
t_u	Thickness of the masonry unit as used in the construction of masonry
v_{el}	Vertical displacement corresponding to the load F_{el}
A_s	Cross sectional area of the specimen parallel to the bed joints (shear test)
E_1	Secant elastic modulus of masonry subject to a compressive loading perpendicular to the bed joints, evaluated at 1/3 of the maximum stress

E_2	Secant elastic modulus of masonry subject to a compressive loading perpendicular to the bed joints, evaluated at 1/10 of the maximum stress
E_3	Chord elastic modulus of masonry subject to a compressive loading perpendicular to the bed joints, evaluated at between 1/10 and 1/3 of the maximum stress
$E_{1,h}$	Secant elastic modulus of masonry subject to a compressive loading parallel to the bed joints, evaluated at 1/3 of the maximum stress
$E_{2,h}$	Secant elastic modulus of masonry subject to a compressive loading parallel to the bed joints, evaluated at 1/10 of the maximum stress
$E_{3,h}$	Chord elastic modulus of masonry subject to a compressive loading parallel to the bed joints, evaluated at between 1/10 and 1/3 of the maximum stress
E_{bt}	Chord elastic modulus of masonry unit subjected to the bending load
F_1	Applied vertical load (bond-wrench test)
F_2	Vertical load due to the weight of the top clamping system (bond-wrench test)
F_3	Vertical load due to the top masonry unit (bond-wrench test)
F_{el}	Selected vertical load value in the linear elastic stage (flexural test of masonry unit)
$F_{\max}$	Maximum vertical load
F_p	Applied lateral pre-compression force (shear test)
G_{f-c}	Fracture energy in compression for loading perpendicular to the bed joints
$G_{f-c,h}$	Fracture energy in compression for loading parallel to the bed joints
G_{fII}	Mode II fracture energy in shear
G_{fx1}	Fracture energy in out-of-plane bending for loading direction parallel to the bed joints
G_{fx2}	Fracture energy in out-of-plane bending for loading direction perpendicular to the bed joints
G_{fx3}	Fracture energy in bending for loading with the moment vector orthogonal to the plane of the wall
$M_{\max}$	Maximum bending moment
W	Section modulus
I	Moment of inertia of the masonry unit along the cross-section

2.2 Abbreviations

Avg.	Average
C.o.V.	Coefficient of variation
St. dev.	Standard deviation
LVDT	Linear variable differential transformer
CS	Calcium silicate
Y.o.C	Year of construction
Vert.	Vertical
Horiz.	Horizontal
IP	In-plane bending

3 Overview of the houses tested in 2016/2017

In this section, an overview of the houses proposed for URM sampling in the testing campaign of 2016/2017 is provided.

Table 2 lists the tested houses indicating the location, the type of building and the year of construction (Y.o.C.). The aim is to provide a complete characterisation of each object whenever possible. The extraction was carried out under the supervision of ARUP. The specimens were delivered at the laboratory of TU Delft and were tested according to testing protocol [5].

The status of the samples upon arrival is shown in Appendix A. During the extraction procedure, many samples were disintegrated. Additionally, from the houses located at Kwelder 1 (KWE-H1) and Hoofdstraat 51 (HOOF-H), the extraction of large size samples was not possible and only individual bricks were extracted. For the house located at Hoofdstraat 51 (HOOF-H1), the extraction took place but no samples were delivered at laboratory of TU Delft. For the building located at Tilweg 24 (TIL) the construction was started in 1990 and completed in 2009 by the owner of the building; a precise year of construction could not be identified for each masonry type thus both years are indicated (1990/2009) for this house.

It should be noted that the samples extracted from the building located at Hogeweg 6 (HOG-H1) showed evidence of joints' repointing.

The specimens were sawn-cut and packed according to the protocol proposed by ARUP [6]. Following this protocol, the samples should have been stripped before shipping to laboratory. However, many samples were covered with plaster, which was removed prior to testing. During this process, 4 out of 10 triplet specimens (TIL-H1-SH) were significantly damaged. One specimen for out-of-plane tests (HOG-H-OOP1) was disintegrated during the handling (see Appendix A).

Table 2 – Overview of proposed houses for extraction of samples [3].

Photo				
Code	HOOF-H	HOG-H	TIL-H	KWE-H
Address	Hoofdstraat 51	Hogeweg 6	Tilweg 24	Kwelder 1
City	't Zandt	Eenum	Oosternieland	Loppersum
Type	Detached	Detached	Detached	Detached
Y.o.C	1907	1912	1990/2009	1995

Table 3 – Overview of delivered samples at TU Delft laboratory.

Code of sample		Masonry type (Y.o.C)	Nr sample	Note	Testing
HOOF-H1	B	Solid clay (1907)	12	*Samples were not delivered*	
HOG-H1	OOP1	Solid clay (1912)	1	Disintegration of sample during preparation	
	OOP2		1	Sample arrived in good condition	Horizontal out-of-plane test
	B		12	Some covered with mortar	Bending and compression test on brick
TIL-H1	CV	CS (1990-2009)	3	Sample covered with plaster	Vertical compression test
	CH		3	Sample covered with plaster	Horizontal compression test
	SH		10	Sample covered with plaster	Shear-compression test
TIL-H2	OOP1	Perforated clay (1990-2009)	3	Sample arrived in good condition	Vertical out-of-plane test
	OOP2		3	Sample arrived in good condition	Horizontal out-of-plane test
	IP		3	Sample arrived in good condition	In-plane bending test
	B		12	Sample covered with mortar	Bending and compression test on brick
KWE-H1	B	CS (1995)	12	Samples arrived in good condition	Bending and compression test on brick

4 Compressive strength of masonry unit

The compressive strength of a masonry unit (brick) is determined in agreement with EN 772-1:2000 [7].

4.1 Testing procedure

To estimate the compressive strength of masonry unit a single masonry unit having a length l_u, a height h_u and thickness t_u was subjected to compression load in agreement with EN 772-1:2000 [7], Figure 1. The compressive test of masonry unit was performed on three types of bricks as follows: solid clay brick (HOG-H), perforated clay brick (TIL-H2) and calcium-silicate brick (KWE-H1).

Figure 1 – Compressive test on a single brick.

The test was carried out through a displacement-controlled apparatus including a hydraulic jack with 300-ton capacity. The hydraulic jack lifts a steel plate, the active side, and there is a passive load plate at the top. A hinge between the load cell and the top steel plate reduces possible eccentricities during loading. A load cell that measures the applied force is attached to the top steel plate. The masonry unit specimens were loaded in such a way that the bed joint plane was perpendicular to the loading direction.
To reach the failure load within 2 min [7], the rate of the jack displacement was set as follows: 0.03 mm/s for solid clay brick, 0.02 mm/s for perforated clay brick and 0.015 mm/s for CS brick.

4.2 Experimental results

The compressive strength of the masonry unit f_b^* can be determined from test on single masonry unit as:

$$f_b^* = \frac{F_{\max}}{l_u . t_u} \tag{1}$$

where F_{max} is the maximum load, l_u and t_u are the length and thickness of the masonry unit respectively.
Following the Annex A of standard EN 772-1 [7], the normalised compressive strength of the masonry unit f_b is determined as:

$$f_b = \delta \cdot f_b^* \tag{2}$$

where δ is the shape factor determined in agreement with Table A.1 in Ref. [7].

Table 4 and Table 5 list the density, the mean and the normalised compressive strength of clay bricks and CS bricks, respectively. The density and normalised compressive strength of the perforated clay bricks used after 1945 is respectively, 1.3 and 3.5 times higher than the compressive strength of the solid bricks used before 1920.
The normalised compressive strength of the clay bricks and CS bricks in terms of histogram representation is shown in Figure 3 and Figure 4, respectively.

Table 4 – Compressive strength of solid clay masonry unit (Y.o.C<1920) and perforated clay masonry unit (Y.o.C>1945).

Solid clay brick- Construction 1912					Perforated clay brick- Construction 1990/2009				
Specimen code	ρ	f^*_b	δ	f_b	Specimen code	ρ	f^*_b	δ	f_b
	Kg/m³	MPa	-	MPa		Kg/m³	MPa	-	MPa
HOG-H-B_A	1658	15.69	0.727	12.08	TIL-H2-B_A	1973	57.25	0.756	43.28
HOG-H-B_B	1583	15.36	0.725	10.86	TIL-H2-B_B	1947	69.19	0.757	52.37
HOG-H-B_C	1580	16.67	0.721	11.78	TIL-H2-B_C	2079	51.57	0.745	38.42
HOG-H-B_D	1618	19.75	0.722	13.96	TIL-H2-B_D	2072	48.61	0.735	35.73
HOG-H-B_E	1553	20.90	0.727	14.78	TIL-H2-B_E	1939	69.84	0.749	52.31
HOG-H-B_F	1594	14.28	0.7255	10.10	TIL-H2-B_F	1979	47.47	0.748	35.51
Ave.	**1598**	**17.11**	**0.724**	**12.26**	**Ave.**	**1998**	**57.32**	**0.748**	**42.94**
St. dev.	**36**	**2.63**	**0.002**	**1.80**	**St. dev.**	**62**	**10.04**	**0.008**	**7.81**
C.O.V.	**0.02**	**0.15**	**0.003**	**0.15**	**C.O.V.**	**0.03**	**0.18**	**0.011**	**0.18**

Table 5 - Compressive strength of the CS masonry unit (Y.o.C>1985).

Calcium silicate brick- Construction 1995				
Specimen code	ρ	f^*_b	δ	f_b
	Kg/m³	MPa	-	MPa
KWB-H_A	1743	17.95	0.880	15.80
KWB-H _B	1766	19.04	0.880	16.75
KWB-H _C	1744	18.28	0.880	16.09
KWB-H _D	1773	19.28	0.880	16.97
KWB-H _E	1752	22.13	0.880	19.47
KWB-H _F	1792	18.25	0.876	15.99
Ave.	**1762**	**19.15**	**0.88**	**16.84**
St. dev.	**19**	**1.54**	**0.002**	**1.37**
C.O.V.	**0.01**	**0.08**	**0.002**	**0.08**

HOG-H
222x55x110-mm

TIL-H2
215x50x100-mm

KWE-H1
215x50x100-mm

Figure 2 – An overview of average dimensions of the masonry unit (brick).

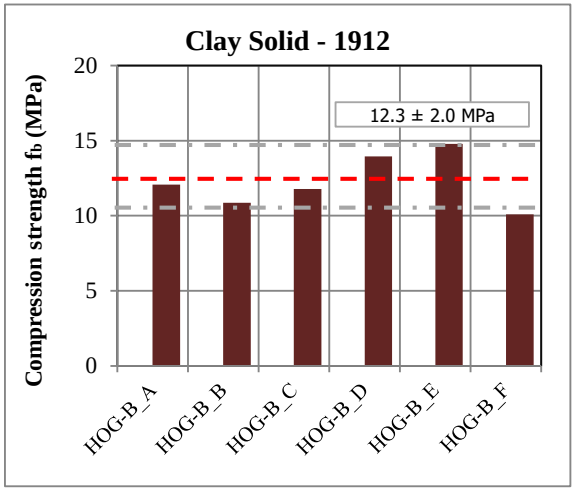

(a)

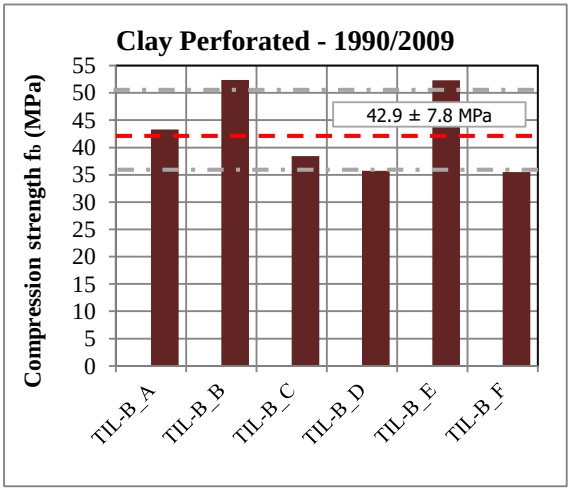

(b)

Figure 3 – Histogram representation of the normalised compressive strength of clay bricks: (a) solid clay bricks used before 1920; (b) perforated clay bricks used after 1945.

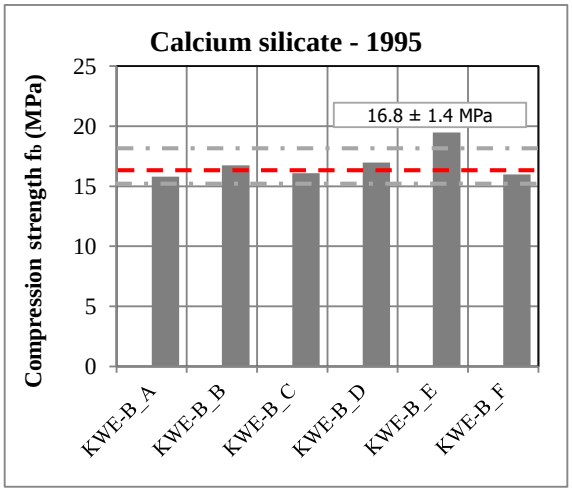

Figure 4 – Histogram representation of the normalised compressive strength of CS bricks used after 1985.

5 Flexural strength of masonry unit

The flexure strength of the masonry unit was determined with three-point bending test following NEN 6790:2005 [8]. The test was also used to determine the elastic modulus of the masonry unit.

5.1 Testing procedure

The masonry units were tested by having the bed joint plane parallel to the loading direction (Figure 5). The specimen was supported by two roller bearings, which were placed 10 mm from the end of the specimen. A third roller was used to apply load to the specimen at mid-span.

The test was carried out by a displacement-controlled apparatus including a hydraulic jack with 100 kN capacity. A spherical joint, between the upper roller and hydraulic jack, was used to minimise load eccentricity. To obtain the failure of the specimen in 30 to 90 s, a displacement rate of 0.02 mm/s was adopted. The applied load was recorded from the load cell attached to the hydraulic jack.

Four LVDTs were attached to the specimens to measure horizontal and vertical displacements. On each side vertical displacement at mid-span of the masonry unit, relative to its supports and elongation between the two points on the masonry unit were measured. The LVDTs had a measuring range of 10 mm with an accuracy of 0.1%.
The measuring system in the current testing campaign was improved, by which a better understanding of the softening post-peak behaviour of masonry unit could be gained. The average value of the crack opening obtained by horizontal LVDTs was used as a control parameter.

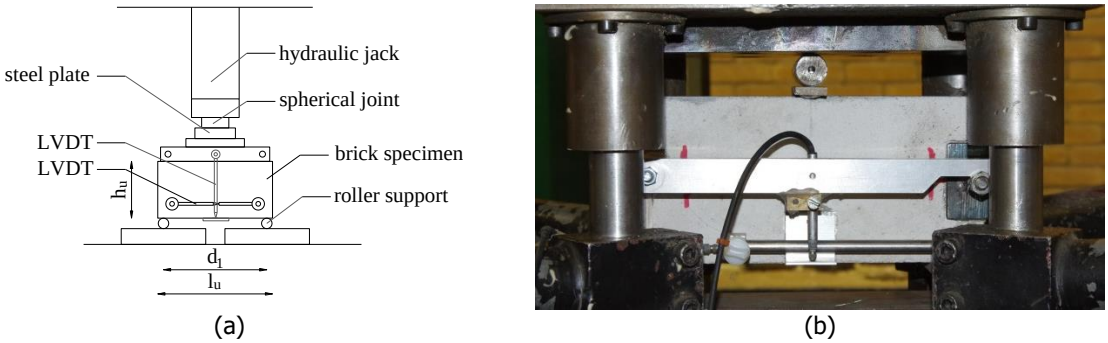

(a) (b)

Figure 5 – Three-point bending test on masonry unit.

5.2 Experimental results

The flexural strength of the masonry unit f_{bt} was determined as:

$$f_{bt} = \frac{3}{2}\frac{F_{\max} d_1}{h_u t_u^2} \tag{3}$$

where F_{max} is the maximum load, d_1 is the distance between the supports, h_u is the height of the masonry unit, t_u is the thickness of the masonry unit.

Assuming a linear stress distribution over the height of the brick's cross-section, the elastic modulus E_{bt} of the masonry units can be determined as follows:

$$E_{bt} = \frac{F_{el} d_1^3}{48 v_{el} I} \tag{4}$$

where F_{el} and v_{el} are the load and vertical displacement in the linear elastic stage, respectively and I is the moment of inertia of the masonry unit along the cross-section.

Figure 6 shows the displacement-force diagram for the three different masonry units. The solid clay bricks showed a linear behaviour up to the peak followed by a brittle failure. The perforated clay bricks and CS bricks showed linear behaviour approximately until 90% of the peak load followed by a post-peak exponential softening.
Table 6 and Table 7 list the density, flexural strength and the Young's modulus of the clay bricks and CS bricks, respectively. The results of flexural strength in terms of histogram are shown in Figure 7 and Figure 8. The perforated clay brick and calcium silicate bricks showed a low variation in strength with an average flexural strength of 5.0 and 3.2 MPa, respectively. A higher variation of flexural strength for the solid clay brick was observed.
The typical observed crack pattern of the tested bricks is shown in Figure 9.

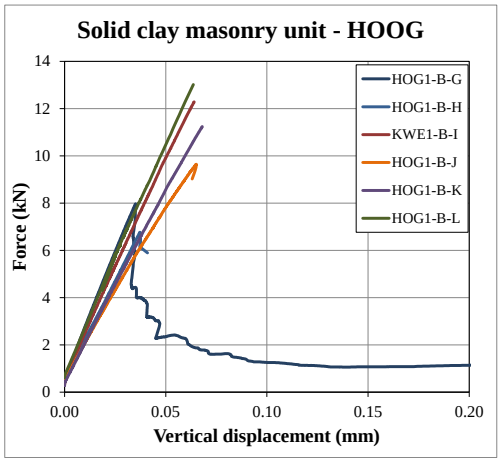

(a)

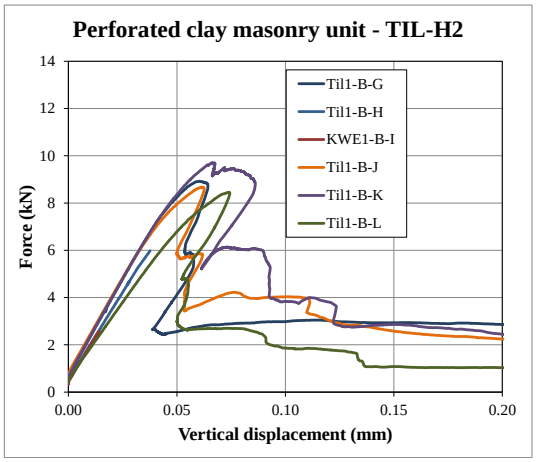

(b)

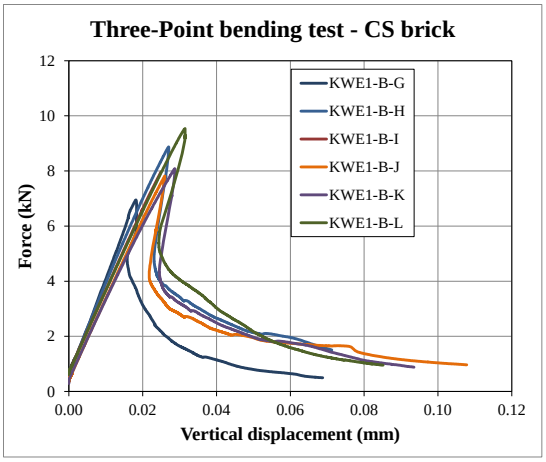

(c)

Figure 6 - Force-vertical displacements curves (LVDTs readings) of three-point bending test on masonry unit: (a) solid clay brick; (b) perforated clay brick; (c) calcium silicate brick.

Table 6 – Flexural strength of solid clay masonry unit (Y.O.C<1920) and perforated clay masonry unit (Y.O.C>1945).

Solid clay brick- Construction 1912				Perforated clay brick- Construction 1990/2009			
Specimen code	ρ Kg/m³	f_{bt} MPa	E_{bt} MPa	Specimen code	ρ Kg/m³	f_{bt} MPa	E_{bt} MPa
HOG-B_G	1630	3.50	5968	TIL-2-B_G	1702	5.22	6217
HOG-B_H	1638	3.14	4544	TIL-2-B_H	1732	3.72	5934
HOG-B_I	1645	5.52	5350	TIL-2-B_I	1643	5.24	5313
HOG-B_J	1602	4.22	4148	TIL-2-B_J	1667	4.97	5909
HOG-B_K	1627	4.90	4482	TIL-2-B_K	1698	5.68	6203
HOG-B_L	1679	5.95	5612	TIL-2-B_L	1667	5.05	5229
Ave.	**1637**	**4.54**	**5017**	**Ave.**	**1685**	**4.98**	**5801**
St. dev.	**25**	**1.12**	**726**	**St. dev.**	**32**	**0.66**	**431**
C.O.V.	**0.02**	**0.25**	**0.14**	**C.O.V.**	**0.02**	**0.13**	**0.07**

Table 7 - Flexural strength of the CS masonry unit (Y.O.C>1985).

Calcium silicate brick- Construction 1995			
Specimen code	ρ Kg/m³	f_{bt} MPa	E_{bt} MPa
KWB-H_G	1733	2.65	7196
KWB-H _H	1733	3.35	7585
KWB-H _I	1722	3.51	7132
KWB-H _J	1747	2.88	6636
KWB-H _K	1775	3.10	6910
KWB-H _L	1714	3.64	6909
Ave.	**1737**	**3.19**	**7062**
St. dev.	**22**	**0.38**	**324**
C.O.V.	**0.01**	**0.12**	**0.05**

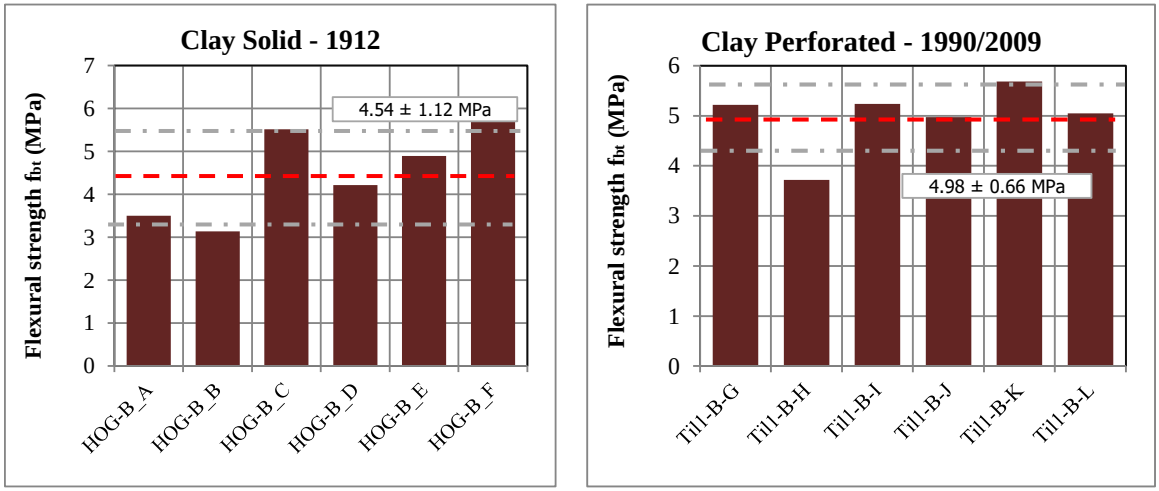

(a) (b)

Figure 7 – Histogram representation of the flexural strength of clay bricks: (a) solid clay bricks used before 1920; (b) perforated clay bricks used after 1945.

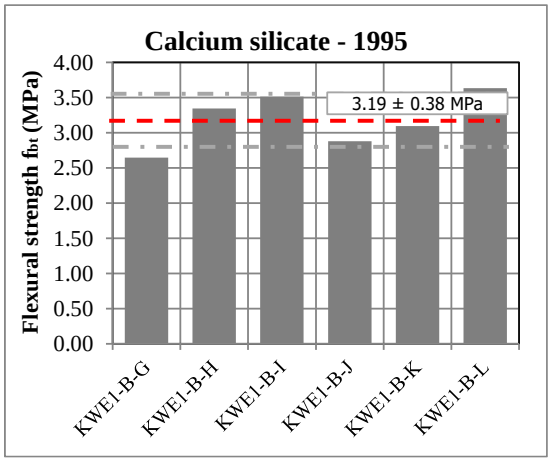

Figure 8 – Histogram representation of the flexural strength of CS bricks used after 1985.

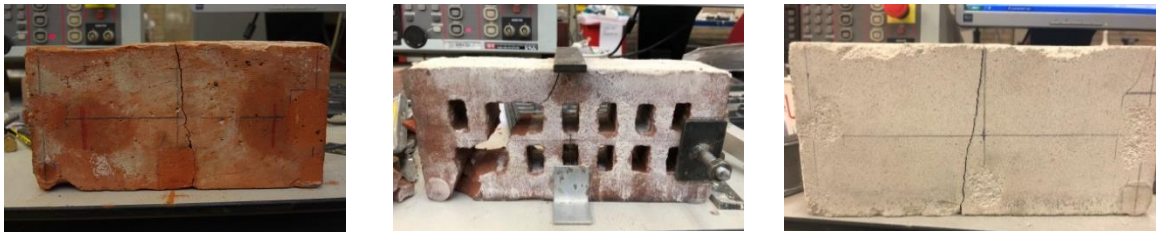

(a) (b) (c)

Figure 9 – Crack pattern of brick: (a) solid clay brick; (b) perforated clay brick; (c) CS brick.

6 Density of masonry

The weight and dimensions of the arrived specimens were measured prior to testing. The average values of the density of masonry for each building are reported in Table 8 to Table 10. The highest density was obtained for perforated clay brick masonry constructed after 1945, while the lowest value was obtained for solid clay brick masonry constructed before 1920.

Table 8 – Density of solid clay brick masonry (HOG-H) used before 1920.

Sample name	Mass	Length	Height	Thickness	Density
	Kg	mm	mm	mm	Kg/m^3
HOG-OOP2-C	39.96	918	340	90	1423
Average					**1423**
Standard deviation					**-**
Coefficient of variation					**-**

Table 9 – Density of perforated clay brick masonry (TIL-H2) used after 1945.

Sample name	Mass	Length	Height	Thickness	Density
	Kg	mm	mm	mm	Kg/m^3
TIL2-OOP1-A	46	419	597	100	1857
TIL2-OOP1-B	52	469	591	100	1862
TIL2-OOP1-C	48	420	595	100	1924
TIL2-OOP2-A	39	933	222	100	1904
TIL2-OOP2-B	41	935	240	100	1824
TIL2-OOP2-C	41	940	226	100	1921
TIL2-IP-A	42	940	230	100	1928
TIL2-IP-B	41	935	241	100	1814
TIL2-IP-C	41	935	242	100	1806
Average					**1871**
Standard deviation					**49**
Coefficient of variation					**0.03**

Table 10 – Density of CS brick masonry (TIL-H1) used after 1985.

Sample name	Mass	Length	Height	Thickness	Density
	Kg	mm	mm	mm	Kg/m^3
TIL-H1-CV-A	39	470	540	101	1502
TIL-H1-CV-B	37	449	512	101	1572
TIL-H1-CV-C	37	449	520	101	1578
TIL-H1-CH-A	39	463	489	101	1714
TIL-H1-CH-B	40	460	493	101	1735
TIL-H1-CH-C	40	461	500	100	1754
TIL-H1-SH1-A	10	238	258	102	1547
TIL-H1-SH1-C	9	225	262	102	1556
TIL-H1-SH1-E	10	267	236	100	1552
TIL-H1-SH1-G	9	250	234	100	1564
TIL-H1-SH1-I	9	255	222	100	1632
TIL-H1-SH1-J	9	223	265	102	1559
Average					**1605**
Standard deviation					**83**
Coefficient of variation					**0.05**

7 Compression properties of masonry

The compression strength and elastic modulus of the masonry were determined in agreement with EN 1052-1:1998 [9]. The orthotropic behaviour of the masonry was investigated. Totally, six CS brick masonry specimens extracted from one object (TIL-H1) were tested.

7.1 Testing procedure

The compression strength and elastic modulus of the masonry were determined in two orthogonal directions with respect to the bed joints. Two configurations were used: a *vertical configuration* in which the loading was perpendicular to the bed joints and a *horizontal configuration* in which the loading was parallel to the bed joint. The former is prescribed by the standard EN 1052-1:1998, while the latter is additionally used to investigate the orthotropic behaviour of the material.

The dimensions of the CS brick specimens as well as LVDT's location for both vertical and horizontal compression tests are reported in Figure 10.

Six LVDTs (three for each side) were attached to the specimen to register vertical relative displacements over the height of the specimen. They were installed as closely as possible to the surface of the specimen to reduce possible errors caused by rotation of the contact points to which they were attached. To monitor the vertical deformation the length of the LVDTs were increased with respect to the one suggested by the standard. A longer length was used in order to capture the entire behaviour of the wallets, with particular attention to the estimation of the fracture energy. The measuring range of the LVDTs was 10 mm with an accuracy of 0.1%. Additionally, two LVDTs (one for each side) were attached to the specimen to register the horizontal relative displacement over the length of the specimen. Their measuring range was 2 mm with an accuracy of 0.1%.

A 10-mm thick layer of gypsum was applied to faces in contact with the loading plates, to ensure that the loaded faces of the specimens were levelled and parallel to one another. This was done to provide even force distribution and prevent unwanted stress concentration in the specimen.

The testing apparatus was provided with a 3000 kN hydraulic jack, positioned at the bottom. The hydraulic jack lifts a steel plate, the active side, and there is a passive load plate at the top. A hinge between the load cell and the top steel plate reduces possible eccentricities during loading. The hydraulic jack is operated in deformation control, using the displacement of the jack as control variable. A load cell that measures the applied force is attached to the top steel plate; see Figure 11.

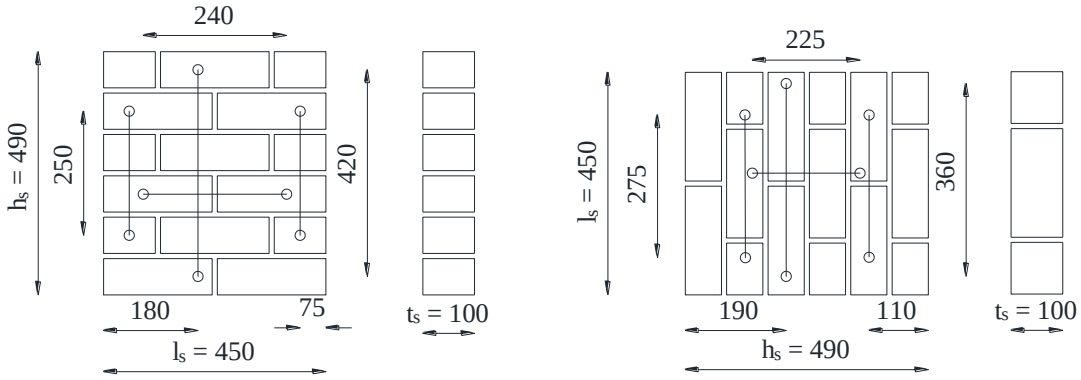

(a) (b)

Figure 10 – Dimensions of the CS brick masonry specimens (TIL-H1): (a) vertical compression test (TIL-H1-CV); (b) horizontal compression test (TIL-H1-CH).

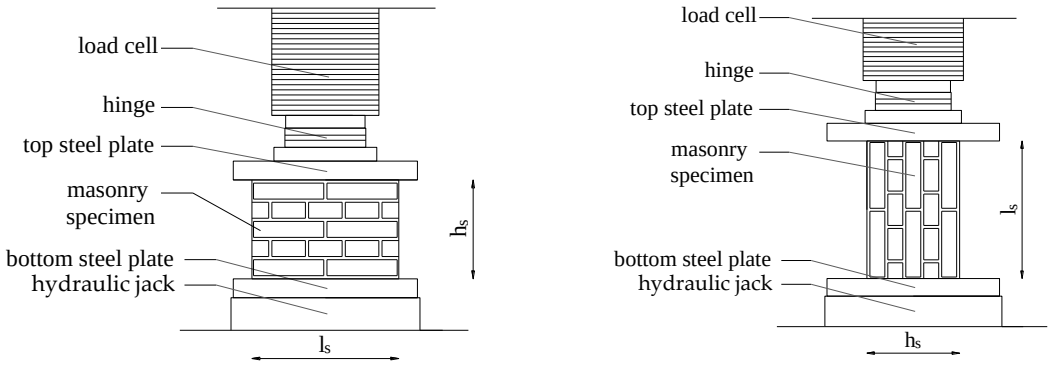

Figure 11 – Test set-up used to compress TIL-H1-CV and TIL-H1-CH specimens: (a) vertical configuration; (b) horizontal configuration.

For the two vertical and horizontal configurations, three specimens were tested by applying a *monotonic loading* as prescribed by the EN 1052-1:1998 [9] (Figure 12). Half of the expected maximum compression force was applied in three equal steps and was kept constant for 2 ± 1 min. Afterwards, the maximum stress was reached monotonically. Subsequently, the test was continued to explore the post-peak behaviour. The load was applied with a rate of 0.003 mm/s to reach the peak stress in 15 to 30 min. The deformation and the force were registered, including the post-peak softening regime.

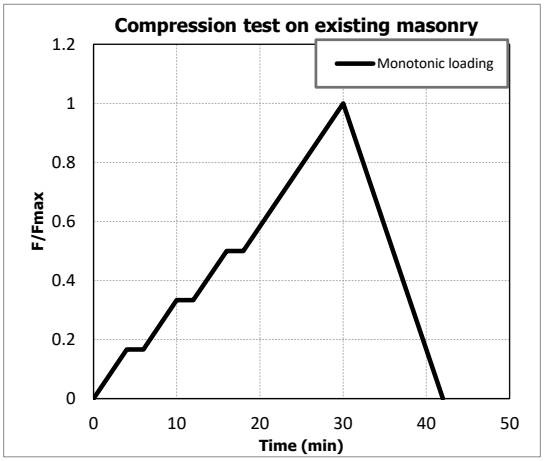

Figure 12 – Monotonic loading scheme for compression test on existing masonry specimen.

7.2 Experimental results

Assuming that the stress is constant over the cross-section of the specimen, the compressive strength of masonry for the vertical, f'_m, and horizontal, $f'_{m,h}$, configuration can be determined as follows:

$$f_m^{'} = \frac{F_{\max}}{t_s l_s} \quad (5)$$

$$f_{m,h}^{'} = \frac{F_{\max}}{t_s h_s} \quad (6)$$

where F_{max} is the maximum load, l_s, h_s and t_s are the dimensions of the masonry specimen as shown in Figure 11.

During the test the displacements and the force were measured continuously allowing the determination of the stress-strain relationship along the loading direction, which was defined as normal direction. From this relation was possible to determine the elastic modulus of masonry. Three estimates of the elastic modulus were adopted (Figure 13a):

- E_1 ($E_{1,h}$) is the secant elastic modulus evaluated at 1/3 of the maximum stress;
- E_2 ($E_{2,h}$) is the secant elastic modulus evaluated at 1/10 of the maximum stress;
- E_3 ($E_{3,h}$) is the chord elastic modulus evaluated between 1/10 and 1/3 of the maximum stress.

The first estimate was consistent with the prescription of EN 1052-1:1998. The third estimate aimed to exclude the initial start-up of the stress-strain diagram, which would unrealistically affects the other two secant estimates with the initial lower slope.

The Poisson ratio v is determined in the elastic phase as the ratio between the lateral strains, which are evaluated in the direction perpendicular to the loading one, and the normal strains (Figure 13 b).

The displacement control procedure of the test allowed determining the post-peak behaviour of the material. The fracture energy in compression $G_{f\text{-}c}$ ($G_{f\text{-}c,h}$) was determined as the area underneath the normal stress versus normal strain diagram, taking the height of the specimen into account. This concept was introduced by van Mier [10] for concrete material and subsequently applied to masonry by Lourenco [11].

The strain obtained by LVDTs' readings and by the jack's readings resulted similar in the post-peak phase. Consequently, the former were used to evaluate the pre-peak phase, while the latter were used to describe the post-peak phase, in which LVDTs may be detached from the specimen due to extensive cracking. The elastic modulus and the Poisson ratio were calculated on the basis of the LVDTs readings, while the fracture energy was calculated on the basis of the LVDTs' reading in the pre-peak phase and jack's reading in the post-peak phase.
The strain associated with peak strength, which is called peak strain, ε_p ($\varepsilon_{p,h}$), is reported in the current document.

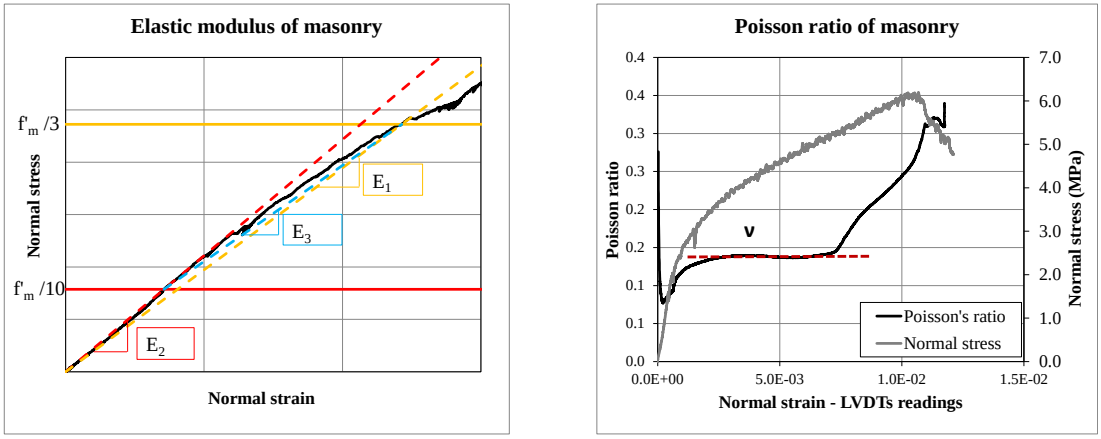

Figure 13 – Compression test on masonry: (a) three estimates of the elastic modulus; (b) evaluation of Poisson ratio.

Figure 14 and Figure 15 show the stress-strain diagram for the CS brick masonry specimens tested under the vertical (TIL-H1-CV) and the horizontal (TIL-H1-CH) configuration, respectively. The graphs refer to the normal direction that is defined as the one parallel to the loading direction. For both configurations, the stress-strain relationship in the normal direction presents a similar trend. The pre-peak stage was characterised by linear-elastic followed by an hardening behaviour until the peak. After the peak stress was reached, a linear softening behaviour was observed for both configurations.

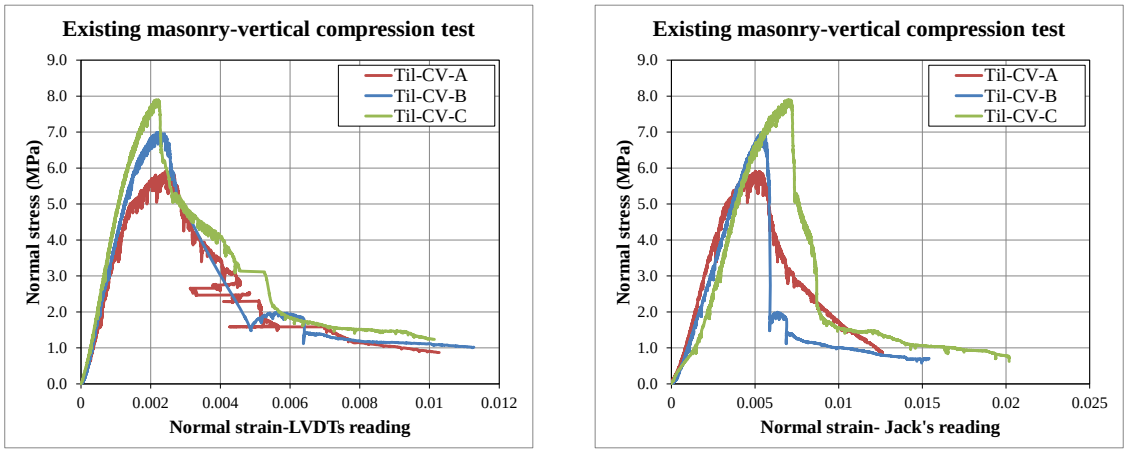

(a) (b)

Figure 14 – Vertical compression tests on CS brick masonry specimens used after 1985 (TIL-H1-CV): (a) normal strain obtained by LVDT's reading; (b) normal strain obtained by jack's reading.

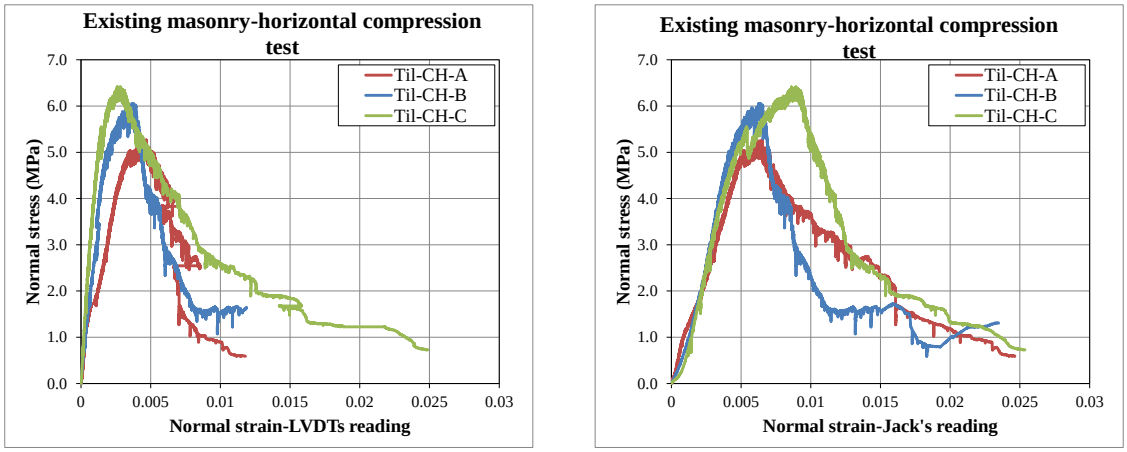

(a) (b)

Figure 15 – Horizontal compression tests on CS brick masonry specimens used after 1985 (TIL-H1-CH): (a) normal strain obtained by LVDT's reading; (b) normal strain obtained by jack's reading.

Figure 16 and Figure 17 analyse the development of cracks in the two specimens tested under vertical and horizontal compression loading, respectively. In case of vertical configuration cracks started in the bricks (Figure 16a), while for horizontal configuration cracks mainly accumulated in the brick-mortar interface (Figure 17a). By increasing the applied load, cracks developed through the thickness of the specimen (Figure 16b and Figure 17b). In the post-peak phase, the specimens showed different behaviour under the two testing configurations. For the case of vertical configuration, the vertical cracks mainly occurred in the bricks and developed uniformly through the length of the specimen (Figure 16c, Figure 16d). For the horizontal configuration, the cracks developed through the height of the specimen, creating a buckling mechanism eventually followed by cracking of the masonry unit (Figure 17c, Figure 17d).

σ_n= 5.31MPa ε_n=1.35‰ (a) σ_p= 6.99MPa ε_p=2.21‰ (b) σ_n= 1.42MPa ε_n=6.45‰ (c) σ_n= 0.71MPa ε_n=11.3‰ (d)

Figure 16 – Crack pattern of CS brick masonry specimen (TIL-H1-CV-B) tested under vertical compression: (a) first crack; (b) maximum stress; (c)-(d) post-peak phase.

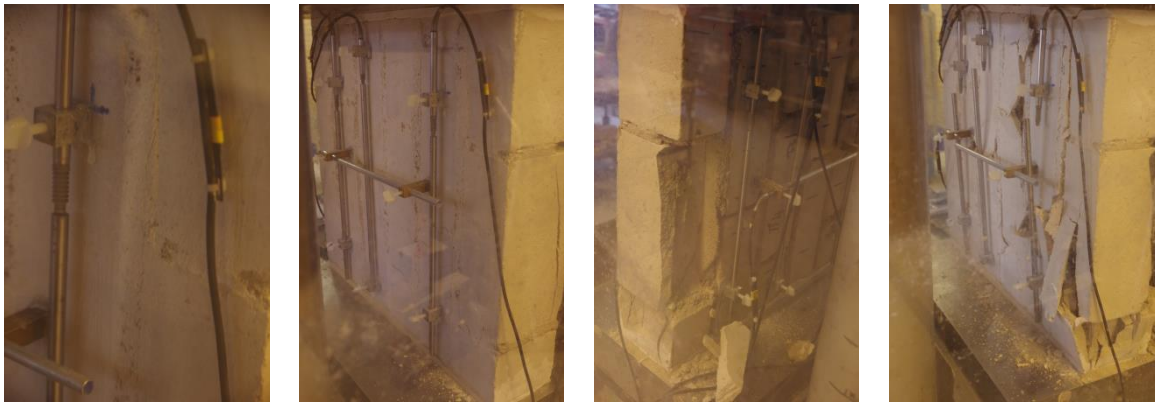

σ_n= 3.19MPa ε_n=1.22‰ (a) σ_p= 6.06MPa ε_p=3.72‰ (b) σ_n= 2.72MPa ε_n=6.04‰ (c) σ_n= 0.82MPa ε_n=12.9‰ (d)

Figure 17 – Crack pattern of CS brick masonry specimen (TIL-H1-CH-B) tested under horizontal compression: (a) first crack; (b) maximum stress; (c)-(d) post-peak phase.

Table 11 and Table 12 list the main experimental results for the CS brick masonry specimens (TIL-H1) subjected to vertical and horizontal compression loading, respectively. The compressive strength, Young's modulus, strain corresponding to the peak strength, fracture energy and Poisson ratio are given. The results in terms of histogram representation are shown in Figure 18 and Figure 19. Although only three specimens per configuration were tested, a lower coefficient of variation is obtained for the compression strength, the strain at peak and the fracture energy in compression; large variation is obtained for the elastic modulus especially for the horizontal configuration.

The orthotropic behaviour of CS brick masonry (TIL-H1) in compression is reported in Table 13. In terms of compressive strength in the two orthogonal directions, no significant variation was found, although vertical configuration showed slightly higher strength (f'_m / $f'_{m,h}$ = 1.2). On the contrary, the peak strain was two times larger in the horizontal direction with respect to the vertical direction (ε_p/ $\varepsilon_{p,h}$ = 0.52). As a result, lower stiffness (E_3 / $E_{3,h}$ = 1.28) and higher values of fracture energy ($G_{f\text{-}c}$ / $G_{f\text{-}c,h}$ = 0.58) were obtained in the horizontal direction. By analysing the crack pattern, it was possible to note that when specimen was rotated and the masonry bed joints coincided with the loading direction, bricks and head joints formed small columns that were subjected to buckling rather than cracking in the bricks.

Table 11 – Results of vertical compression tests on CS brick masonry constructed after 1985 (TIL-H1-CV).

Specimen name	Year of construction	f'_m	E_1	E_2	E_3	ε_p	$G_{f\text{-}c}$	ν
		MPa	MPa	MPa	MPa	‰	N/mm	-
TIL-H1-CV-A	1990-2009	5.91	3244	2400	3938	2.43	15.49	-
TIL-H1-CV-B		6.99	3717	2725	4545	2.21	11.28	0.13
TIL-H1-CV-C		7.90	4360	3532	4939	2.17	16.80	0.13
Average		**6.93**	**3774**	**2886**	**4474**	**2.27**	**14.52**	**0.13**
Standard deviation		**1.00**	**560**	**583**	**504**	**0.14**	**2.88**	**0.00**
Coefficient of variation		**0.14**	**0.15**	**0.20**	**0.11**	**0.06**	**0.20**	**0.01**

Table 12 – Results of horizontal compression tests on CS brick masonry constructed after 1985 (TIL-H1-CH).

Specimen name	Year of construction	$f'_{m,h}$	$E_{1,h}$	$E_{2,h}$	$E_{3,h}$	$\varepsilon_{p,h}$	$G_{f\text{-}c,h}$	ν_h
		MPa	MPa	MPa	MPa	‰	N/mm	-
TIL-1-CH-A	1990-2009	5.27	2499	2814	2367	4.44	26.48	-
TIL-1-CH-B		6.06	3065	3314	2953	3.72	24.50	-
TIL-1CH-C		6.42	5004	4697	5173	2.81	23.67	-
Average		**5.92**	**3523**	**3608**	**3498**	**3.66**	**24.88**	**-**
Standard deviation		**0.59**	**1314**	**975**	**1480**	**0.81**	**1.44**	**-**
Coefficient of variation		**0.10**	**0.37**	**0.27**	**0.42**	**0.22**	**0.06**	**-**

Table 13 – Orthotropic behaviour of CS brick masonry (TIL-H1) subjected to compression loading.

Year of construction 1990-2009 (TIL-H1)	f'_m $f'_{m,h}$	E_1 $E_{1,h}$	E_2 $E_{2,h}$	E_3 $E_{3,h}$	ε_p $\varepsilon_{p,h}$	$G_{f\text{-}c}$ $G_{f\text{-}c,h}$
	MPa	MPa	MPa	MPa	‰	N/mm
Vertical configuration	6.93	3774	2886	4474	2.27	14.52
Horizontal configuration	5.92	3523	3608	3498	3.66	24.88
Ratio Vertical/Horizontal	**1.17**	**1.07**	**0.80**	**1.28**	**0.62**	**0.58**

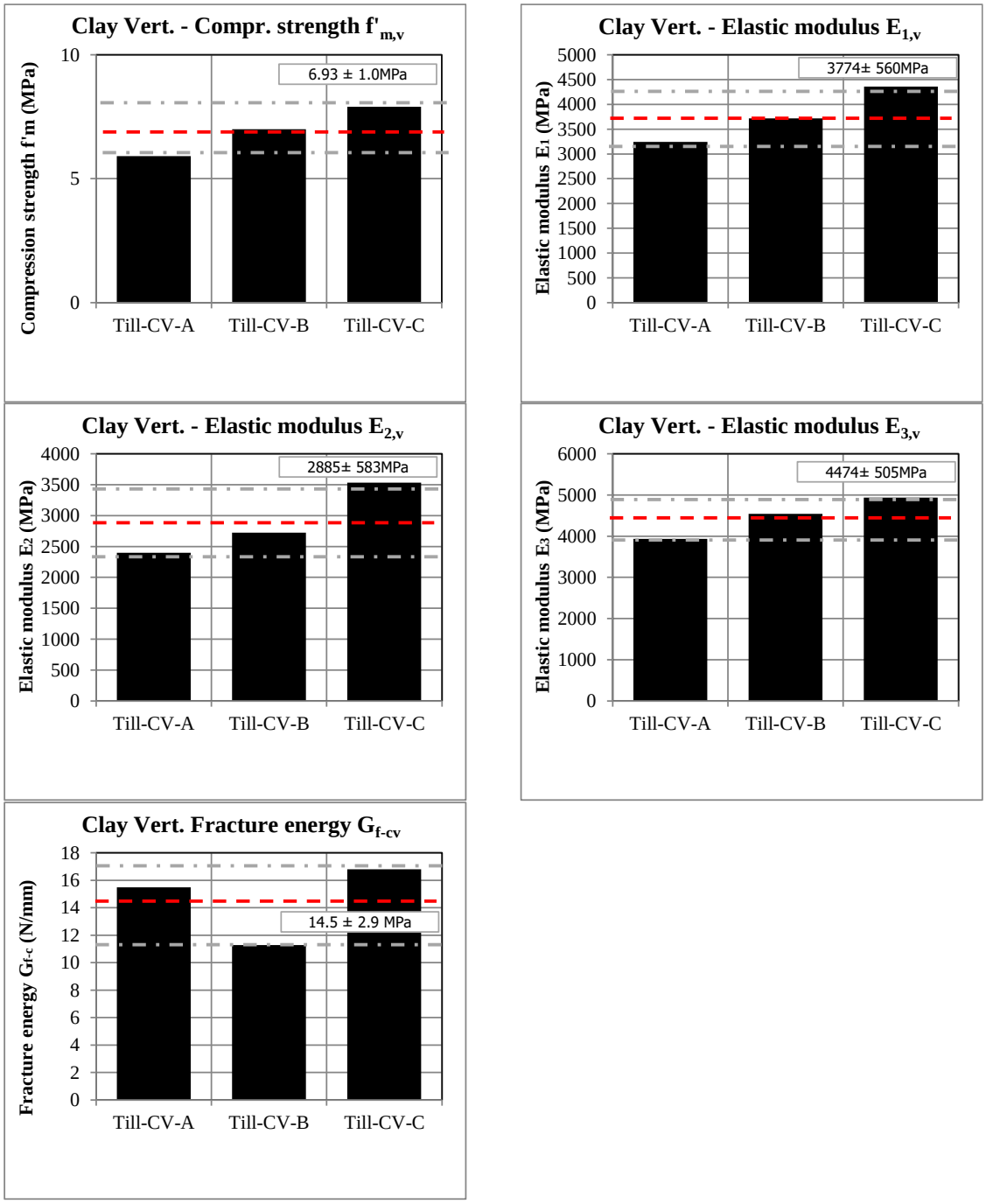

Figure 18 – Vertical compression tests on CS brick masonry constructed after 1985 (TIL-H1-CV): histogram representation.

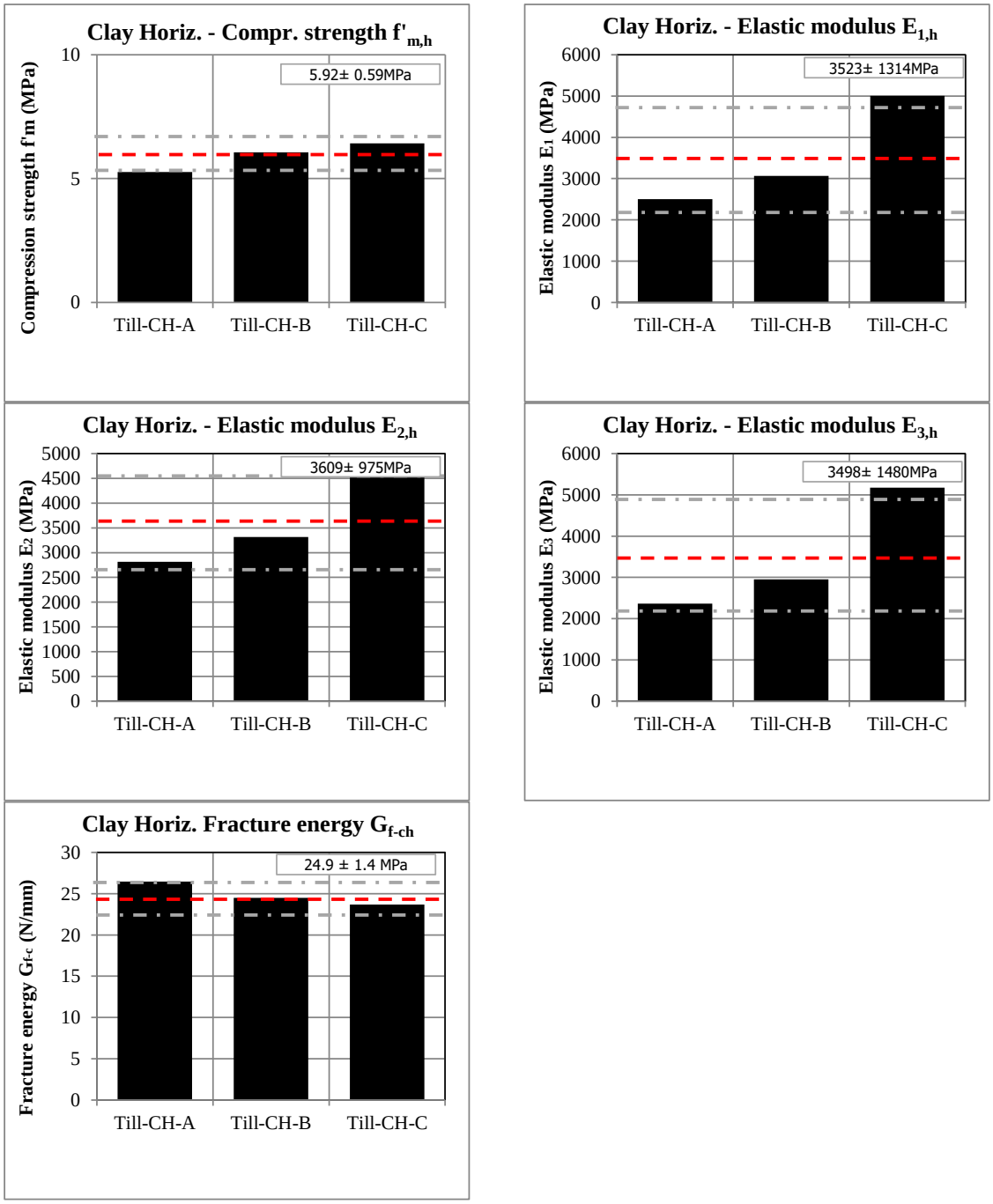

Figure 19 – Horizontal compression tests on CS brick masonry constructed after 1985 (TIL-H1-CH): histogram representation.

8 Flexural strength of masonry

The flexural strength of masonry was determined for three configurations:

- Four-point bending test with the moment vector parallel to the bed joints and in the plane of the wall, which generates a plane of failure parallel to the bed joints (denoted as vertical out-of-plane bending test OOP1);
- Four-point bending with the moment vector orthogonal to the bed joints and in the plane of the wall, which generates a plane of failure perpendicular to the bed joints (denoted as horizontal out-of-plane bending test OOP2);
- Four-point bending with the moment vector orthogonal to plane of the wall (denoted as in-plane vertical bending test IP).

The first two tests were performed in agreement with EN 1052-2:1999 [12], while the third one was a no-standardized test.

8.1 Testing procedure

The masonry specimens tested with the moment vector in the plane of the wallets were designed in agreement with EN 1052-2:1999 [12]. An overview of dimensions of the tested specimens is listed in Table 14. The masonry type, the dimensions and the distance between the bearing supports d_1 and loading supports d_2 are listed.

Table 14 – Overview of dimensions of specimens adopted for bending tests.

Type of test	Code of sample	Number of sample	Dimension (brick)	l_s (mm)	h_s (mm)	d_1 (mm)	d_2 (mm)
Vertical out-of-plane bending	TIL-H2-OOP1	3	2x10	595	420	420	220
Horizontal out-of-plane bending	TIL-H2-OOP2	3	4x4	940	240	660	360
	HOG-H1-OOP2	1	4x5	920	340	660	360
In-plane bending test	TIL-H2-IP	3	4x4	940	240	660	360

In the current testing campaign, a new test set-up for the out-of-plane bending tests was designed, as shown in Figure 20. In the improved set-up, the specimens were placed vertically and loaded in such a way that the bending axis was always horizontal. Consequently, the contribution of the masonry self-weight was excluded.

The load was applied via cylindrical roller bearings mounted to steel hollow profiles with springs, which enabled them to easily move. A counterweight was used to minimise the friction forces between the specimen and the loading support, the loading support was suspended using steel wire. The bearing rollers were mounted to the test rig with springs. The distance between the loading, d_2, and bearing rollers, d_1, was chosen according to the standard (Table 14). At the base, the specimen was supported by a steel plate positioned on top of a flat ball bearings.

The load was applied in displacement control by a spherical joint attached to a hydraulic jack with 100 kN capacity. The applied load was recorded from the load cell attached to the hydraulic jack. For each side, a maximum of five LVDTs was attached to measure the vertical and horizontal displacements in the constant moment zone (Figure 20). The LVDTs had a measuring range of 10 mm with an accuracy of 0.1%. Apart from the test set-up, the measuring system was also improved, by which a better understanding on the softening post-peak behaviour of masonry could be gained. In this view, two vertical LVDTs were installed on the back face of the specimen to measure the crack opening. The average value of the crack opening obtained by these LVDTs was used as a control parameter.

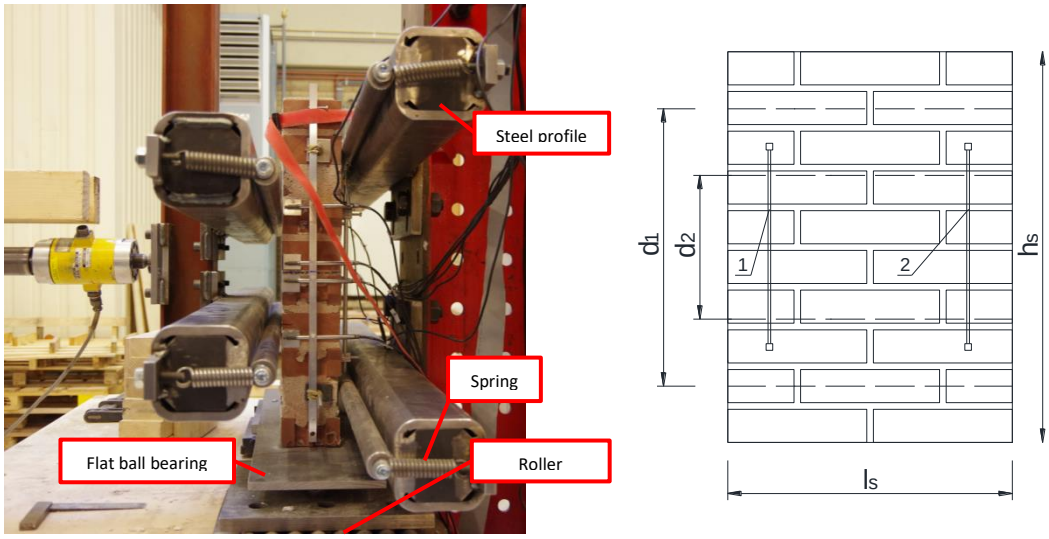

(a) (b)

Figure 20 – Out-of-plane bending: (a) testing set-up; (b) average of LVDTs reading used as control parameter.

Figure 21 shows the in-plane bending test set-up. The load was applied in displacement control by a spherical joint attached to a hydraulic jack with 100 kN capacity. The applied load was recorded from the load cell attached to the hydraulic jack.
The deflection of the specimen in the constant moment zone was measured using five vertical LVDTs on each side. In addition, the crack opening was measured using the horizontal LVDTs; one on each side. The crack opening, obtained as the average value of the two horizontal LVDTs readings, was used as a parameter to control the applied load. Consequently, the load was imposed in order to provide a gradual increase in crack opening at the centre of the wallet.

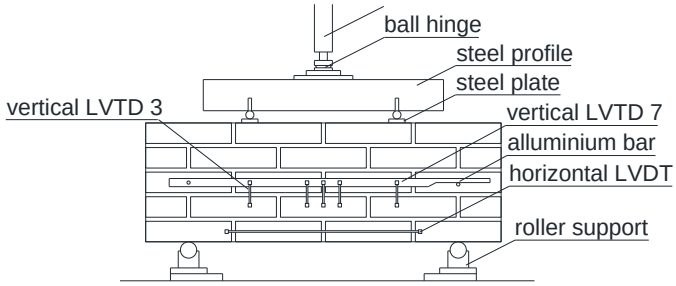

Figure 21 – In-plane bending (IP): testing set-up.

8.2 Experimental results

The flexural strength of the out-of-plane tests can be determined as follows:

$$f_{x1} = \frac{3F_{\max} d_3}{l_s t_s^2} \tag{7}$$

$$f_{x2} = \frac{3F_{\max} d_3}{h_s t_s^2} \tag{8}$$

where F_{max} is the maximum load at failure, d_3 is the distance between the loading and the bearing support, l_s is the length of masonry specimen, h_s is the height of masonry and, t_s is the thickness of masonry specimen.

The flexural strength of the in-plane tests f_{x3} can be determined as follows:

$$f_{x3} = \frac{M_{\max}}{W} = \frac{(F_{\max} d_3 / 2 + p d_1^2 / 8)}{W} \quad (9)$$

where M_{max} is the maximum bending moment, F_{max} is the maximum load at failure, d_3 is the distance between the loading and the bearing support, d_1 is the distance between the bearing support, p is the masonry self-weight uniform load (calculated using a density as described in Section 6) and W is the section modulus.

The concept of fracture energy associated with tensile cracking has already been used for the steel and concrete. Subsequently, this concept was applied to masonry as introduced by Van der Pluijm [13]. Thanks to using improved set-up, the fracture energy determined from the four-point bending test can be calculated as the sum of the areas underneath the two point loads versus the deflection diagram corresponding to these loads, taking into account the cross-section of the specimen. The fracture energy for the vertical out-of-plane bending G_{fx1}, horizontal out-of-plane bending G_{fx2}, and in-plane bending G_{fx3} were calculated.
Figure 22 shows the force versus deflection curve at the loading point used to calculate the fracture energy. In some case, especially for the out-of-plane tests, a plateau was found in the post-peak phase, which might be attributed to the weight of the specimen, formation of mixed cracks propagated along multiple joints and constraining of the specimen after a certain deformation. In this case, the stress-strain relationship adopted for the estimation of the fracture energy was modified by considering a linear approximation of the curve after the peak load. The slope of the post-peak curve calculated between the maximum load and approximately 10% reduction in the maximum load was used as a basis to approximate the post-peak phase (Figure 22a).

Figure 23 shows the force-displacement curve for existing masonry specimens subjected to bending tests. In the case, the installation of a central LVDT was not possible the mid-span displacement has been calculated from the readings of the other LVDTs, by applying a linear interpolation. A post-peak softening behaviour could be observed for almost all the tested specimens.

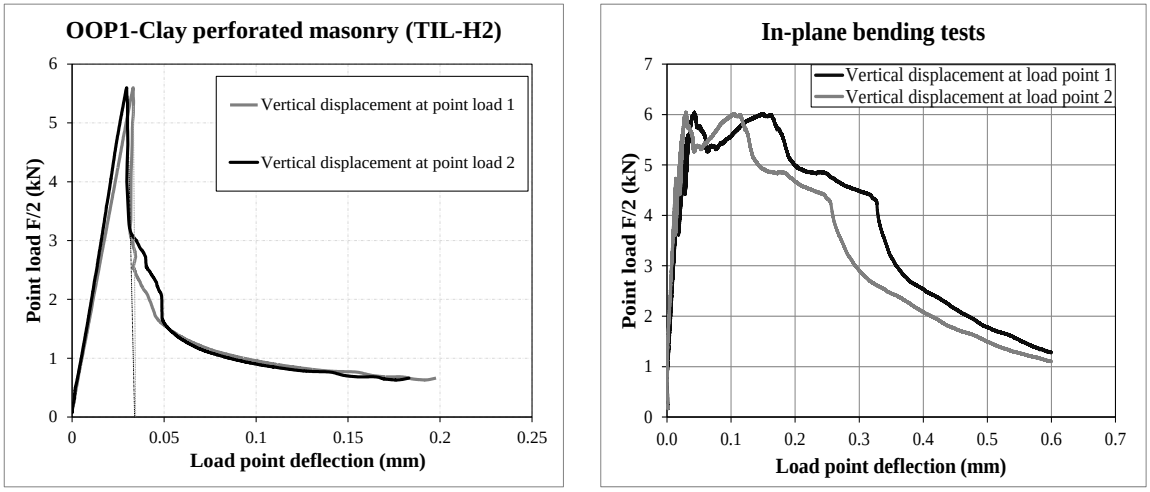

(a) (b)

Figure 22 – Force versus deflection curve at loading point used to calculate the fracture energy: (a) out-of-plane bending; (b) in-plane bending.

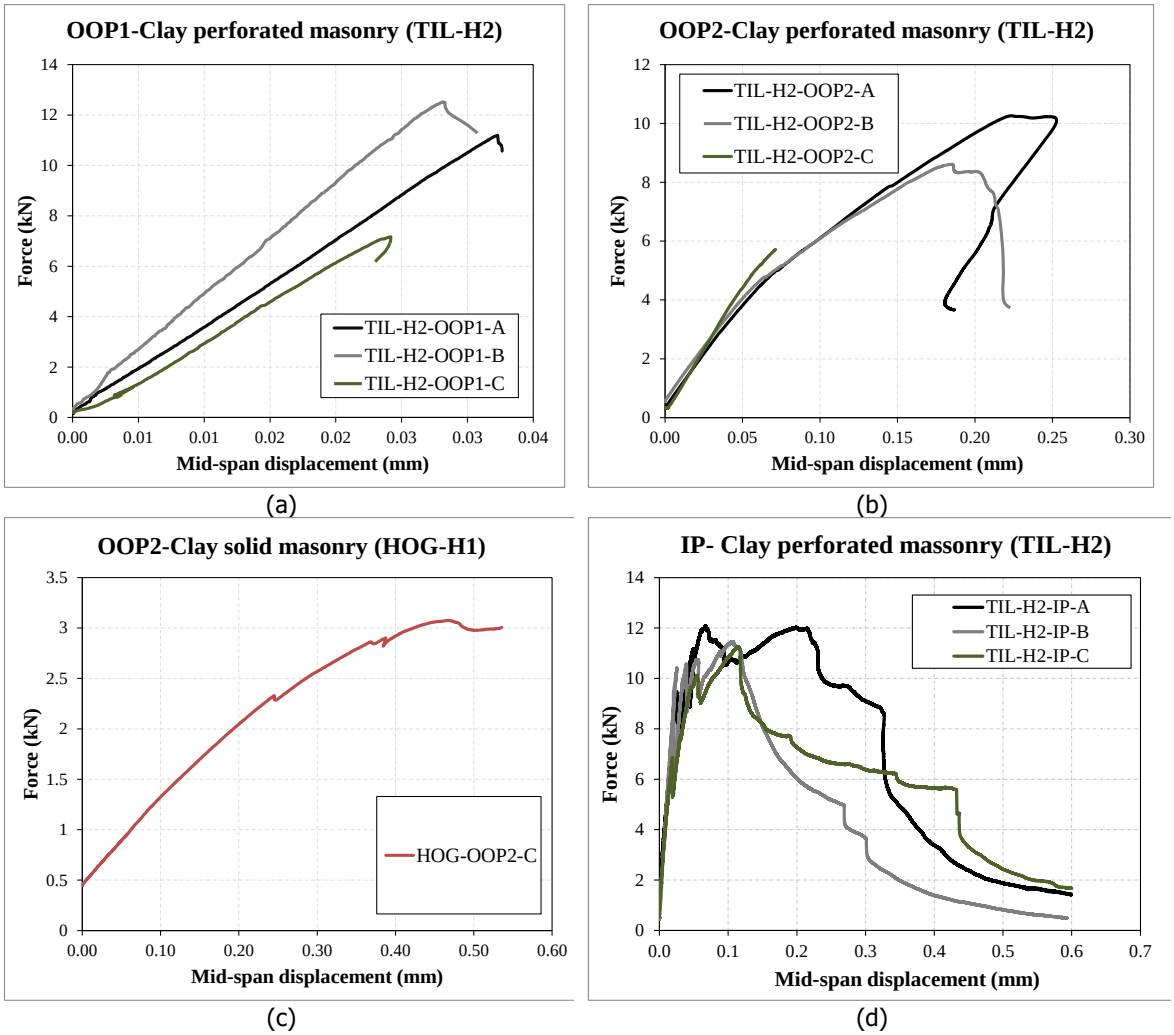

Figure 23 – Force-displacement curve for existing masonry subjected to: (a) vertical out-of-plane bending test on clay perforated masonry (TIL-H2); (b) horizontal out-of-plane bending test on clay perforated masonry (TIL-H2); (c) horizontal out-of-plane bending test on clay solid masonry (HOG-H); (d) in-plane bending on clay perforated masonry (TIL-H2).

The bending properties of the solid clay brick masonry and perforated clay brick masonry specimens in terms of flexural strength and the fracture energy are listed in Table 15 and Table 16, respectively. It should be pointed out that only two specimens made of solid clay bricks (HOG-H) were delivered to the laboratory; one sample to be subjected to the vertical out-of-plane bending (HOG-OOP1) and the other one to be subjected to horizontal out-of-plane bending (HOG-H-OOP2). Due to the weak bond between bricks and mortar, the HOG-OOP1 sample was disintegrated during preparation.

For the perforated clay brick masonry (Table 16), the horizontal out-of-plane flexural strength resulted approximately 2.3 times higher than the vertical out-of-plane flexural strength (f_{x2} / f_{x1} = 2.3). The value of in-plane flexural strength resulted approximately 1.4 times higher than the vertical out-of-plane flexural strength (f_{x3} / f_{x1} = 1.36).

Table 15 – Bending properties of solid clay brick masonry (HOG-H1) constructed before 1920.

Specimen name	Year of construction	f_{x2}	G_{fx2}
		MPa	N/mm
HOG-OOP2-C	**1912**	**0.41**	**0.036**

Table 16 – Bending properties of perforated clay brick masonry (TIL-H2) constructed after 1945.

Specimen name	f_{x1}	G_{fx1}	Specimen name	f_{x2}	G_{fx2}	Specimen name	f_{x3}	G_{fx3}
	MPa	N/mm		MPa	N/mm		MPa	N/mm
TIL-2-OOP1-A	0.80	0.005	TIL-2-OOP2-A	2.08	0.046	TIL-2-IP-A	1.06	0.22
TIL-2-OOP1-B	0.80	0.008	TIL-2-OOP2-B	1.61	0.034	TIL-2-IP-B	0.91	0.19
TIL-2-OOP1-C	0.51	0.002	TIL-2-OOP2-C	1.14	0.013	TIL-2-IP-C	0.89	0.25
Average	**0.70**	**0.005**	**Average**	**1.61**	**0.031**	**Average**	**0.95**	**0.22**
St. dev.	**0.17**	**0.003**	**St. dev.**	**0.47**	**0.017**	**St. dev.**	**0.07**	**0.03**
C.o.V.	**0.24**	**0.53**	**C.o.V.**	**0.29**	**0.55**	**C.o.V.**	**0.08**	**0.14**
			f_{x2} / f_{x1}	**2.3**		f_{x3} / f_{x1}	**1.36**	

The crack patterns of specimens for the bending tests are shown in Figure 24 to Figure 27.
In the vertical out-of-plane bending test, the perforated clay masonry specimens cracked in one bed joint located in the constant moment zone (Figure 24).
In the case of horizontal out-of-plane bending tests, two failure modes were observed as follows (Figure 25):

- Alternating crack running through the head joints and bed joints (TIL-H2-OOP2-A to C).
- Vertical crack in the middle of the sample starting from the mortar and developed upward (HOG-H1-OOP2-C)

For the in-plane bending test (Figure 26), the cracking occurred in both bed and head joints creating a stepwise pattern developed outside the constant moment zone. The cracking of the brick near to the applied load was also reported in two specimens.

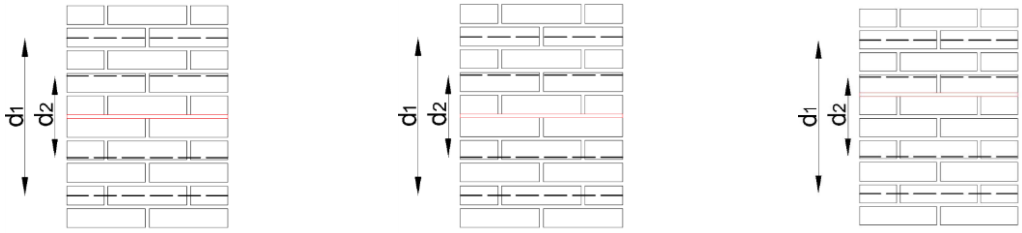

(a) TIL-2-OOP1-A (b) TIL-2-OOP1-B (c) TIL-2-OOP1-C

Figure 24 - Crack pattern of perforated clay brick masonry TIL-H2 specimens subjected to vertical out-of-plane bending (OOP1).

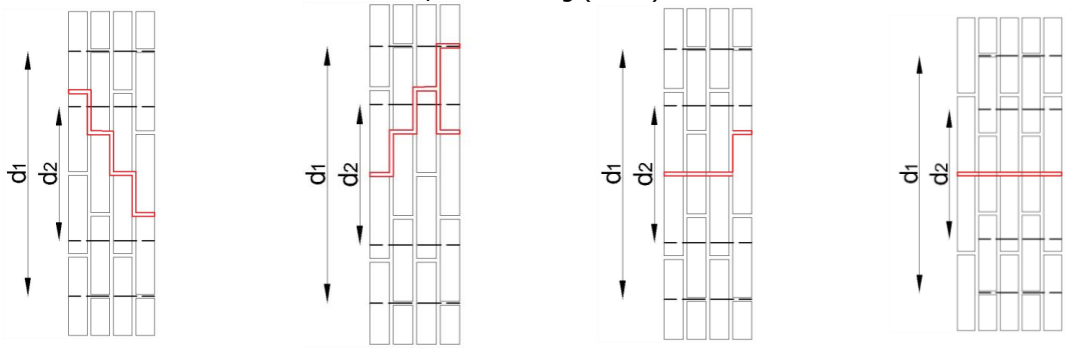

(a) TIL-H2-OOP2-A (b) TIL-H2-OOP2-B (c) TIL-H2-OOP2-C (d) HOG-H1-OOP2-C

Figure 25 - Crack pattern of specimens subjected to horizontal out-of-plane bending: (a)-(c) perforated clay brick masonry (TIL-H2); (d) solid clay brick masonry (HOG-H1).

(a) TIL-H2-IP-A (b) TIL-H2-IP-B

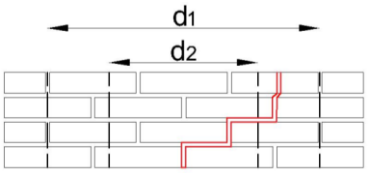

(c) TIL-H2-IP-C

Figure 26 - Crack pattern of perforated brick masonry specimens (TIL-H2) subjected to in-plane bending (IP).

(a)

(b)

(c)

Figure 27 – Crack pattern of existing masonry specimens subjected to four-point bending tests: (a) vertical out-of-plane bending; (b) horizontal out-of-plane bending; (c) in-plane bending.

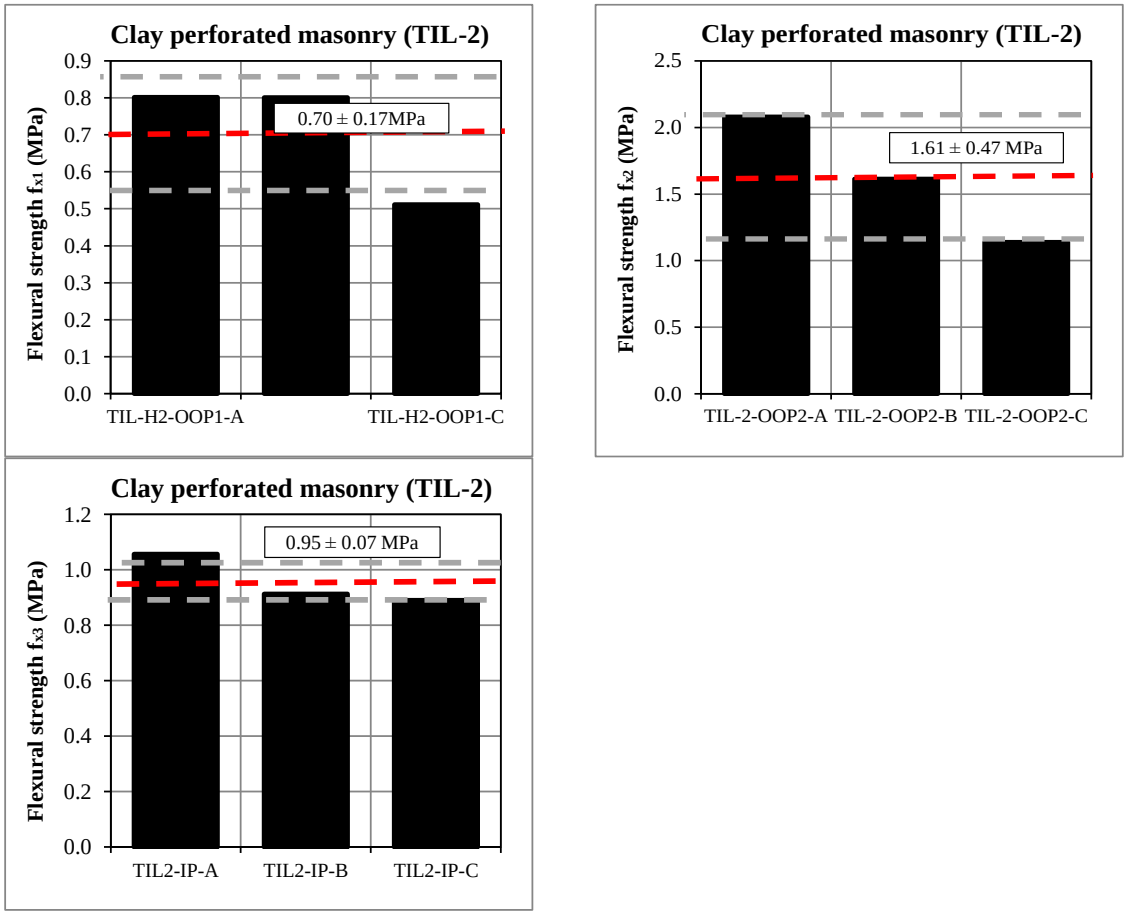

Figure 28 – Bending properties of perforated clay brick masonry specimens constructed after 1945 (TIL-H2): histogram representation.

9 Bond strength of masonry

The bond strength between masonry unit and mortar was determined in agreement with the bond wrench test proposed by EN 1052-5:2002 [14].

9.1 Testing procedure

The couplet specimens were sawn-cut from the specimens previously subjected to the bending test. The solid clay brick masonry (HOG-H1) and perforated clay brick masonry specimens (TIL-H2) were subjected to the bond wrench test.

The improved test set-up is used in this campaign as shown in Figure 29a. The specimen is rigidly held by a support frame that holds the specimen in accordance with EN 1052-5:2005 [14]. A clamp attached to a lever is placed on top of the masonry unit. The lever is used to apply a bending moment to the brick-mortar interface. The load is applied by a jack operated manually and a load cell attached to the jack measures the applied force. Therefore, the improved set-up provides the possibility for recording the applied load continuously.

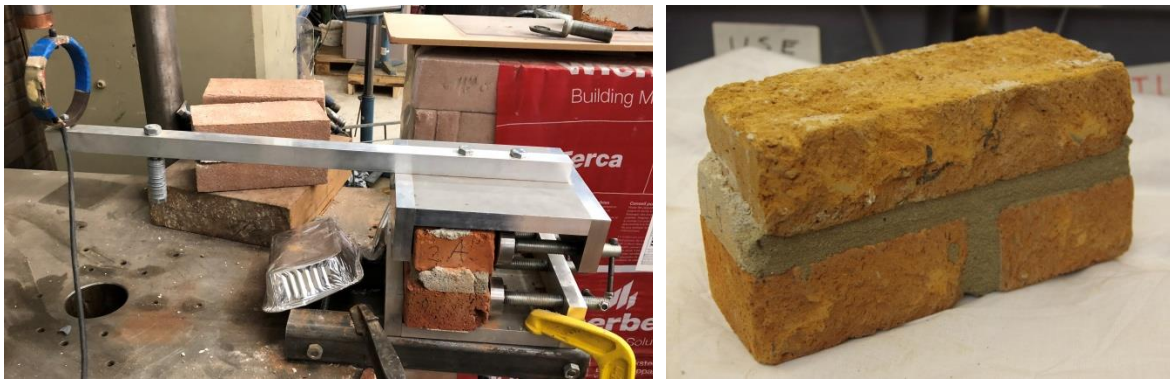

(a) (b)

Figure 29 – Bond wrench tests: (a) improved set-up; (b) sawn-cut couplet specimens.

9.2 Experimental results

The bond wrench strength f_w is calculated on the assumption that the stress distribution is linear over the width of the top masonry unit [14]:

$$f_w = \frac{F_1 e_1 + F_2 e_2 - \frac{2}{3} t_u \left(F_1 + F_2 + \frac{F_3}{4} \right)}{l_j w_j^2 / 6} \tag{10}$$

where F_1 is the failure load, measured and applied by the jack. F_2 is the normal force as a result of the weight of the bond wrench apparatus. F_3 is the weight of the masonry unit pulled off the specimen, including the weight of adherent mortar. Furthermore, e_1 is the distance from the applied load to the tension face of the specimen, e_2 is the distance from the centre of gravity of the clamp to the tension face of the specimen, l_j is the mean length of the bed joint, and w_j is the mean width of the bed joint. Figure 30 shows the set-up and the definition of the various quantities.

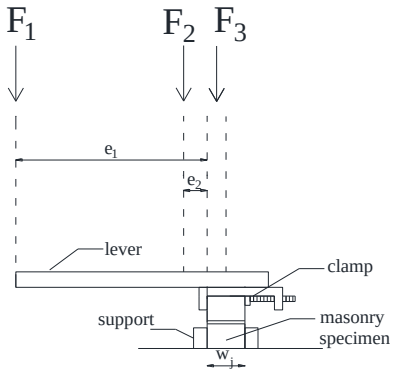

Figure 30 – Test set-up for the bond wrench test.

Figure 31 reports the classification of the type of failures [14], while Figure 32 shows the observed failure mechanisms.

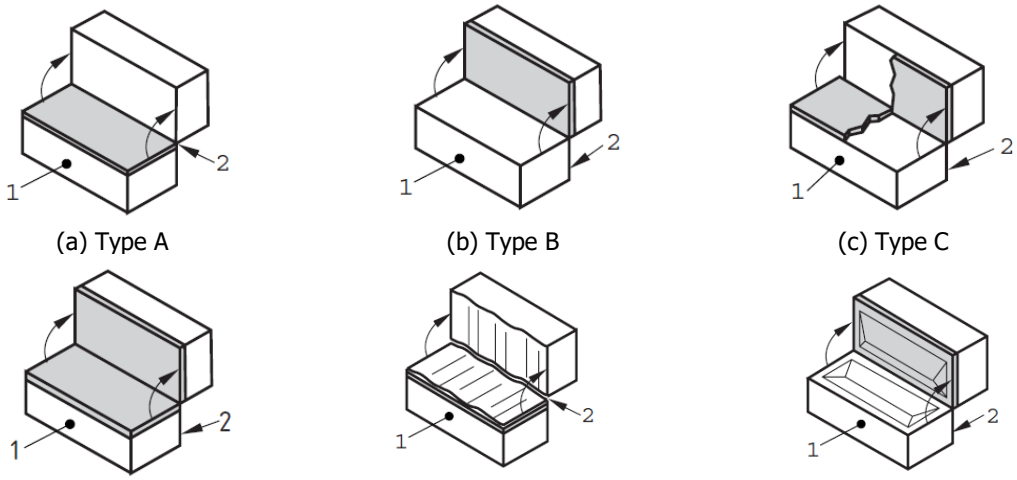

(a) Type A (b) Type B (c) Type C

(d) Type D (e) Type E (f) Type F

Figure 31 – Classification of failure modes in agreement with EN-1052-5:2005 (1 tension face, 2 compression face).

(a) (b)

Figure 32 – Observed failure mechanisms: (a) solid clay brick masonry with joint's repointing (HOG-H1); (b) perforated clay brick masonry (TIL-H2).

Figure 33 shows the applied load (F_1) versus time. All specimens showed brittle behaviour.
Table 17 and Table 18 list the results of bond wrench test on the solid and perforated clay brick masonry, respectively. The bond strength values of specimens in terms of histogram are shown in Figure 34.

From a physical point of view, it may be expected that there is a correlation between the flexural bond tensile strength, f_w, and flexural masonry strength. This correlation depends on loading direction so that the crack plane occurs along the brick to mortar interface in the bed joint plane, f_{x1}. One reason might be the fact that these parameters depend on the adhesion between mortar and brick. A ratio equal to 1.2 is found between the bond strength and the vertical flexural strength obtained from testing of perforated clay brick masonry specimens (TIL-H2).

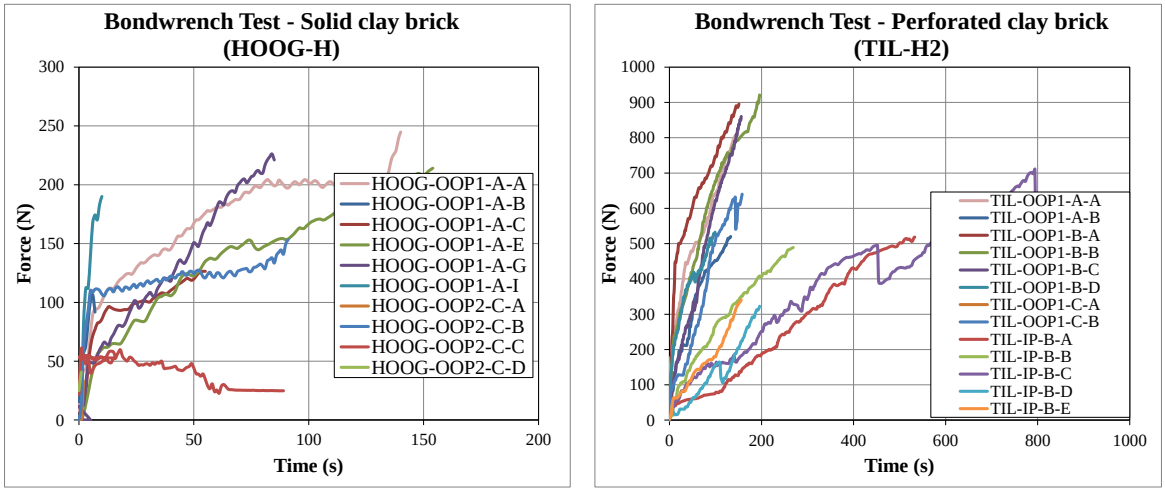

(a) (b)

Figure 33 – Time versus force (F1) applied by manually controlled jack: (a) solid clay brick masonry constructed before 1920 (HOG-H1); (b) perforated clay brick masonry (TIL-H2) constructed after 1945.

Table 17 – Bond strength of solid clay brick masonry samples constructed before 1920 (HOG-H1).

Specimen Name	l_j	w_j	F_3	F_1	f_w
	mm	mm	N	N	MPa
HOG-OOP1-A-A	211	95	13	245	0.33
HOG-OOP1-A-B	210	93	18	107	0.15
HOG-OOP1-A-C	211	96	13	126	0.17
HOG-OOP1-A-E	211	96	12	214	0.29
HOG-OOP1-A-G	214	92	18	226	0.33
HOG-OOP1-A-I	212	96	20	190	0.25
HOG-OOP2-C-A*	210	94	20	63	0.09
HOG-OOP2-C-B	212	96	16	162	0.21
HOG-OOP2-C-C*	211	99	12	60	0.07
HOG-OOP2-C-D*	211	96	16	45	0.06
Average					**0.25**
St. dev.					**0.07**
C.o.V.					**0.29**

*Excluded from the average due to the incorrect application of the load

Table 18 – Bond strength of perforated clay brick masonry samples constructed after 1945 (TIL-H2).

Specimen Name	l_j	w_j	F_3	F_1	f_w
	mm	mm	N	N	MPa
TIL-H2-OOP1-A-A	211	100	23	822	1.01
TIL-H2-OOP1-A-B	215	100	23	567	0.68
TIL-H2-OOP1-B-A	223	101	22	896	1.02
TIL-H2-OOP1-B-B	221	101	23	921	1.06
TIL-H2-OOP1-B-C	219	100	20	860	1.02
TIL-H2-OOP1-B-D	217	102	21	717	0.82
TIL-H2-OOP1-C-A	214	100	21	579	0.70
TIL-H2-OOP1-C-B	214	102	22	640	0.74
TIL-H2-IP-B-A	221	100	26	518	0.61
TIL-H2-IP-B-B	216	100	22	489	0.59
TIL-H2-IP-B-C	220	100	23	712	0.84
TIL-H2-IP-B-D	217	98	21	713	0.89
TIL-H2-IP-B-E	216	99	25	896	1.10
Average					**0.85**
St. dev.					**0.18**
C.o.V.					**0.21**
f_w/f_{x1}					**1.21**

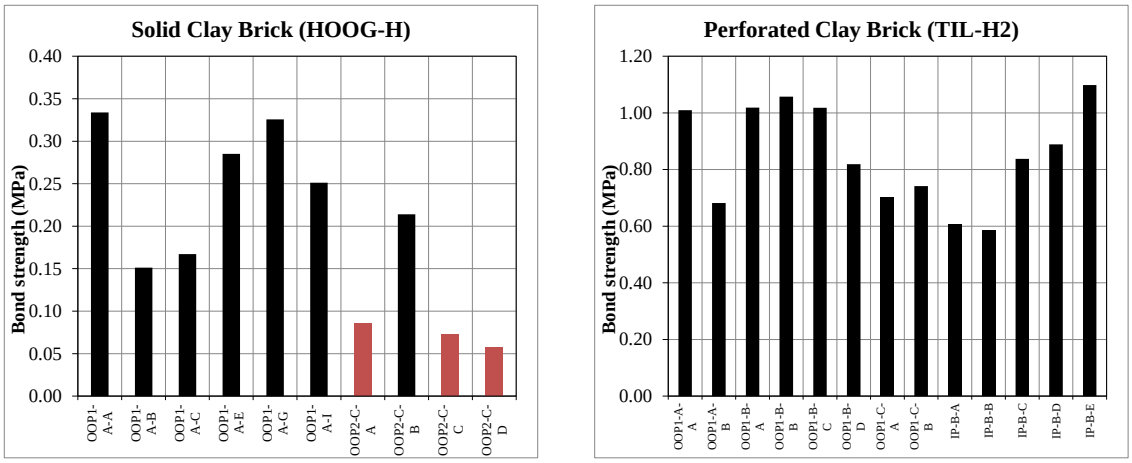

(a) (b)

Figure 34 – Bond strength values of clay brick masonry: histogram representation: (a) solid clay brick masonry constructed before 1920 (HOG-H1); (b) perforated clay brick masonry constructed after 1945 (TIL-H2). In red excluded values.

10 Shear properties of masonry

The initial shear properties of masonry were determined in agreement with EN 1052-3:2002 [15]. However, a displacement control procedure was used, instead of the prescribed force control procedure, to evaluate the residual strength properties and the mode-II fracture energy.

10.1 Testing procedure

Prior to testing, a layer of gypsum was applied to the external faces of the specimens. It should be mentioned that some of the samples were disintegrated during the removal of plaster or preparation and handling, as already mentioned in Section 3. Totally, six specimens were tested.

Figure 35 shows the used test set-up. During the test, the specimen was rotated 90 degrees with respect to the position as it was extracted. The specimen was kept under constant lateral pre-compression, while a shear load was applied at the mid masonry unit. Three different levels of pre-compression were investigated. Being the compressive strength of the masonry unit greater than 10 N/mm^2 [15], the pre-compression stresses applied were 0.2, 0.6 and 1.0 N/mm^2. For each pre-compression level, two samples was tested.

Two independently operated jacks were required to apply the shear and pre-compressive load. The shear load acts in a vertical direction using a displacement controlled apparatus. The apparatus has a 100 kN jack and a spherical joint. The displacement increased with a rate of 0.005 mm/s. The pre-compressive load was applied perpendicular to the bed joint plane by a manually operated hydraulic jack. The horizontal hydraulic jack was load controlled and applied different levels of transverse compressive load to the specimen. The jack was kept in position by means of four steel rods positioned on opposite sides of the specimen, which were kept in position by steel plates (Figure 35a). In order to keep the transverse compressive load constant (with less than 2% change), a spring system is used between the hydraulic jack and the load cell. The stiffness of the springs is defined on the basis of the required pre-compression level. A load cell is placed between the spring and the steel plate to measure the applied load.

Both on the front and the backside of the specimens, LVDTs are attached. Vertical LVDTs measure the relative vertical displacement of the middle brick with respect to the latter ones. Horizontal LVDTs measures the horizontal displacement between the two external bricks. Their measuring range is 10 mm with an accuracy of 0.5% (Figure 35b).

To get more information regarding the post-peak behaviour, a second phase of the test was performed in which the pre-compression load was increased and kept constant in the residual phases. This allows gathering more data for estimation of the failure envelope in the residual phase.

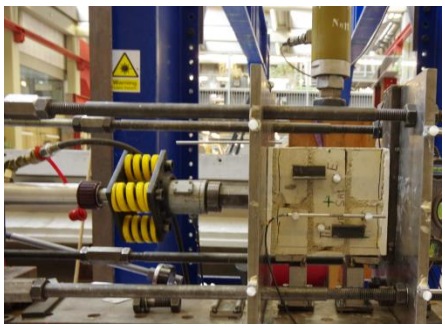

(a)

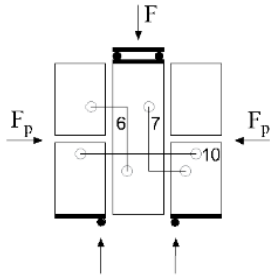

(b)

Figure 35 – Shear-compression test on masonry specimen: (a) test set-up; (b) adopted measuring system.

10.2 Experimental results

The shear strength f_v was calculated for each specimen as follows [14]:

$$f_v = \frac{F_{\max}}{2A_s} \tag{11}$$

where F_{max} is the maximum load, A_s is the cross sectional area of the specimen parallel to the bed joints.

The pre-compression stress f_p can be calculated for each specimen as follows [14]:

$$f_p = \frac{F_p}{A_s} \tag{12}$$

where F_p is the pre-compression force.

The test was carried out in displacement control allowing the determination of the post-peak behaviour. As a consequence, the residual shear strength $f_{v,res}$ was also determined. The residual strength occurred at an almost constant load where a plateau was observed. The resistance in the post-peak phase can be associated to dry friction.

The results of all the tests were plotted in a pre-compressive stress versus shear strength diagram. Considering a linear regression of data, the initial shear strength f_{v0} and the coefficient of friction μ can be found such as the intercept with the vertical axis and the gradient of the line, respectively. The angle of internal friction α was determined as the angle between the regression line and the horizontal axis.
Similar consideration can be applied to determine the residual shear strength $f_{v0,res}$ and the residual coefficient of friction μ_{res}. In the Coulomb friction formulation, the result is:

$$f_v = f_{v0} + \mu f_p \tag{13}$$

$$f_{v,res} = f_{v0,res} + \mu_{res} f_p \tag{14}$$

Tests were performed only on CS brick masonry specimens. The description of status of the CS brick masonry triplets can be found in Appendix A. The specimens were delivered with a layer of plaster. During the removal of plaster and handling, some of the specimens were disintegrated. As a result, only 6 out of 10 specimens were tested, as shown in Figure 36. Among the tested specimens, 3 out of 6 specimens showed damage in both one bed and head joint (TIL-SH1-A and TIL-SH1-J, Figure 36) or only in one bed joint (TIL-SH1-C, Figure 36).

The shear stress versus relative displacement of the central brick of the triplets is shown in Figure 37. The sliding of the middle unit is reported both in terms of LVDTs' reading (max range 10 mm) and in terms of jack's reading. A summary of the results of shear-compression tests for the CS brick masonry specimens constructed after 1985 (TIL-H1) is listed in Table 19.
The shear strength versus pre-compression stress are plotted in Figure 38a. For two specimens (TIL-SH1-I and TIL-SH1-C) the shear strength at the peak and at the residual phase is almost similar, which indicates that the brick-mortar interface was damaged prior to testing. The testing results obtained from testing of TIL-SH1-G specimen substantially deviate from the results of other specimens. The observed anomaly in the shear properties of this sample might be attributed to the difference between the thicknesses of the two bed joints (Figure 36f). As a result, the outcomes of these three specimens are excluded from the evaluation of the shear properties (filled markers in Figure 38a).

Table 20 lists the shear properties of CS brick masonry triplets constructed after 1985 (TIL-H1). The CS brick masonry showed an initial shear strength equal to 0.11 MPa and a coefficient of friction equal to 0.35. The coefficient of friction in the residual phase is almost the same as the one for the initial phase.
All the specimens presented a shear failure in the unit-mortar bond area. Figure 40 shows a typical crack pattern.

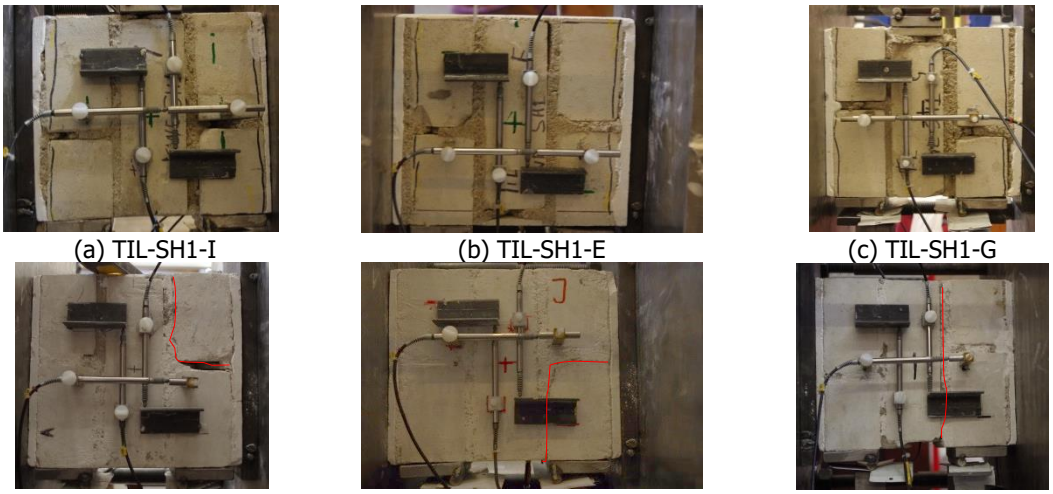

(a) TIL-SH1-I (b) TIL-SH1-E (c) TIL-SH1-G

(d) TIL-SH1-A (e) TIL-SH1-J (f) TIL-SH1-C

Figure 36 – Status of the triplets prior to testing.

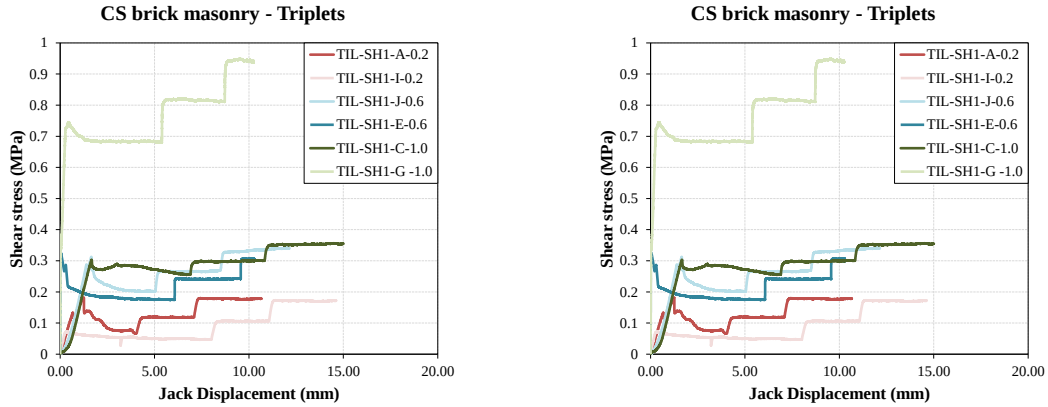

(a) (b)

Figure 37 – Shear stress versus relative displacement of the central brick for CS brick triplets (TIL-H1): (a) Jack' readings; (b) LVDT's readings.

Table 19 – Shear properties for CS brick masonry specimens constructed after 1985 (TIL-H1).

f_p = 0.2 MPa				f_p = 0.6 MPa				f_p = 1.0 MPa			
Specimen name	f_v	$f_{v,res}$	G_{f-II}	**Specimen name**	f_v	$f_{v,res}$	G_{f-II}	**Specimen name**	f_v	$f_{v,res}$	G_{f-II}
	MPa	MPa	N/mm		MPa	MPa	N/mm		MPa	MPa	N/mm
TIL-SH1-I	0.07*	0.05	-	TIL-SH1-E	0.32	0.18	0.049	TIL-SH1-G	0.74*	0.68*	0.037
TIL-SH1-A	0.18	0.08	0.098	TIL-SH1-J	0.31	0.20	0.051	TIL-SH1-C	0.61*	0.51*	-
Average	**0.13**	**0.06**	**0.098**	**Average**	**0.32**	**0.19**	**0.05**	**Average**	**0.52**	**0.48**	**0.037**
St. dev.	**0.08**	**0.02**	**-**	**St. dev.**	**0.01**	**0.02**	**0.00**	**St. dev.**	**0.31**	**0.29**	**-**
C.o.V.	**0.61**	**0.25**	**-**	**C.o.V.**	**0.03**	**0.08**	**0.03**	**C.o.V.**	**0.60**	**0.61**	**-**

* The data are excluded in the calculation of initial shear properties

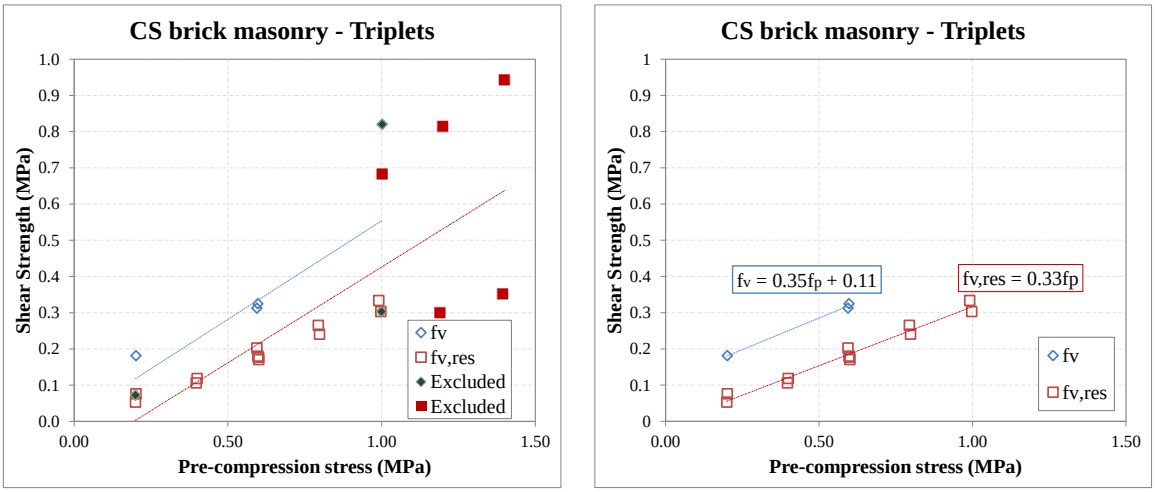

(a) (b)

Figure 38 – Shear strength versus pre-compression stress for CS brick masonry triplets (TIL-H1): (a) all the results with indication of excluded data; (b) data considered for determining the shear properties.

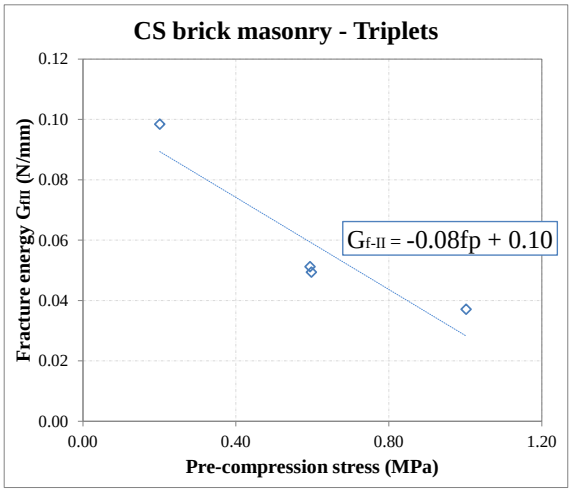

Figure 39 – Mode II-fracture energy versus pre-compression for CS brick masonry triplets (TIL-H1).

Table 20 - Shear properties of CS brick masonry triplets constructed after 1985 (TIL-H1).

Property	Symbol	Unit	Triplets
Number of specimens			6
Initial shear strength	f_{v0}	MPa	0.11
Initial coefficient of friction	μ		0.35
Angle of internal friction	α		19.3
Residual shear strength	$f_{res,v}$	MPa	0
Residual coefficient of friction	μ_{res}		0.33
Residual angle of internal friction	α_{res}		18.3

(a) (b) (c)

Figure 40 - Crack pattern of triplets under shear test: (a) front-left joint; (b) front-right joint; (c) front view.

11 Summary and properties overview

In this report the characterisation of materials extracted from the existing buildings in the large scale testing campaign of 2016 is reported. The experimental results of this campaign aim at enriching the masonry abacus. The testing campaign selected as a case study four detached houses characterised by: 1) solid clay brick masonry constructed before 1920; 2) perforated clay brick masonry constructed after 1945; 3) calcium silicate brick masonry constructed after 1985. Whenever possible, the large samples were extracted and delivered to the laboratory of TU Delft for testing.

Table 21 and Table 22 show an overview of the material properties of clay and calcium silicate brick masonry, respectively. Due to the difficulties raised during sampling, limited specimens were delivered to being subjected to the compression, bending load and shear-compression load. Apart from test on large samples, compression and flexural tests on the masonry units were performed.
The compression tests were performed in two orthogonal directions, perpendicular and parallel to the bed joints, aiming to investigate the orthotropic behaviour of masonry.
The bending properties of the masonry were studied by performing four-point bending tests, both out-of-plane and in-plane, and bond wrench tests. Using the improved testing set-up, horizontal out-of-plane bending tests, where the plane of failure was perpendicular to the bed joints, and vertical out-of-plane bending tests, where the plane of failure was parallel to the bed joints, were performed. In-plane bending test was adopted where the moment vector was orthogonal to the plane of the specimen. In both in-plane and out-of-plane bending tests, the crack opening was used as a controlling parameter allowing an estimation of the post-peak behaviour. The bond wrench tests were performed on the specimens sawn-cut from the remaining parts of those samples previously subjected to the bending load.
The shear properties of masonry were obtained by performing shear-compression tests on triplets. By adopting a displacement-controlled procedure, the initial shear parameters, including initial shear strength and coefficient of friction was studied and the residual strength property, where a plateau was reached, was investigated. The initial and residual shear properties were found by applying Coulomb friction criterion.

Table 21 – Overview of the mechanical properties of clay brick masonry.

Property	Symbol	Unit	Solid clay masonry <1920				Perforated clay >1945			
			Average	St. dev.	C.o.V.	Number of test	**Average**	St. dev.	C.o.V.	Number of test
Normalised compressive strength of masonry unit	f_b	MPa	**12.26**	1.80	0.15	6	**42.94**	7.81	0.18	6
Flexural strength of masonry unit	f_{bt}	MPa	**4.54**	1.12	0.25	6	**4.98**	0.66	0.13	6
Elastic modulus of masonry unit	E_b	MPa	**5017**	726	0.14		**5801**	431	0.07	
Density of masonry	ρ	Kg/m^3	**1423**	-	-	1	**1871**	49	0.03	9
Masonry flexural strength with the moment vector parallel to the bed joints and in the plane of the wall	f_{x1}	MPa	**-**	-	-	0	**0.70**	0.17	0.24	3
Fracture energy in bending with the moment vector parallel to the bed joints and in the plane of the wall	G_{fx1}	N/mm	**-**	-	-		**0.005**	0.003	0.53	
Masonry flexural strength with the moment vector orthogonal to the bed joint and in the plane of the wall	f_{x2}	MPa	**0.41**	-	-	1	**1.61**	0.47	0.29	3
Fracture energy in bending with the moment vector orthogonal to the bed joint and in the plane of the wall	G_{fx2}	N/mm	**0.036**	-	-		**0.031**	0.017	0.55	
Masonry flexural strength with the moment vector orthogonal to the plane of the wall	f_{x3}	MPa	**-**	-	-	0	**0.95**	0.07	0.08	3
Fracture energy in bending with the moment vector orthogonal to the plane of the wall	G_{fx3}	N/mm	**-**	-	-		**0.22**	0.03	0.14	
Flexural bond strength	f_w	MPa	**0.25**	0.07	0.29	7	**0.85**	0.18	0.21	13

Table 22 – Overview of the mechanical properties of CS brick masonry constructed after 1985.

Property	Symbol	Unit	Calcium silicate masonry >1985			
			Average	St. dev.	C.o.V.	Number of test
Normalised compressive strength of masonry unit	f_b	MPa	**16.84**	1.37	0.08	6
Flexural strength of masonry unit	f_{bt}	MPa	**3.19**	0.38	0.12	6
Elastic modulus of masonry unit	E_b	MPa	**7062**	324	0.05	
Density of masonry	ρ	Kg/m^3	**1605**	83	0.05	12
Compressive strength of masonry in the direction perpendicular to bed joints	f'_m	MPa	**6.93**	1.00	0.14	3
Elastic modulus of masonry in the direction perpendicular to bed joints	E_1	MPa	**3774**	560	0.15	
	E_2	MPa	**2886**	583	0.20	
	E_3	MPa	**4474**	504	0.11	
Fracture energy in compression for loading perpendicular to bed joints	$G_{f\text{-}c}$	N/mm	**14.52**	2.88	0.20	
Poisson ratio of masonry in compression for loading perpendicular to bed joints	v	-	**0.13**	0.00	0.01	
Strain corresponding to peak strength in compression for loading perpendicular to bed joints	ε_p	‰	**2.27**	0.14	0.06	
Compressive strength of masonry in the direction parallel to bed joints	$f'_{m,h}$	MPa	**5.92**	0.59	0.10	3
Elastic modulus of masonry in the direction parallel to bed joints	$E_{1,h}$	MPa	**3523**	1314	0.37	
	$E_{2,h}$	MPa	**3608**	975	0.27	
	$E_{3,h}$	MPa	**3498**	1480	0.42	
Fracture energy in compression for loading parallel to bed joints	$G_{f\text{-}c,h}$	N/mm	**24.88**	1.44	0.06	
Strain corresponding to peak strength in compression for loading parallel to bed joints	$\varepsilon_{p,h}$	‰	**3.66**	0.81	0.22	
Masonry (bed joint) initial shear strength	f_{v0}	MPa	**0.11**	**-**	-	3
Masonry (bed joint) initial shear friction coefficient	μ	-	**0.35**	**-**	-	
Residual masonry (bed joint) initial shear strength	$f_{v0,res}$	MPa	**0.00**	**-**	-	
Residual masonry (bed joint) shear friction coefficient	μ_{res}	-	**0.33**	**-**	-	

References

[1] Jafari, S., Panoutsopoulou, L. and Rots, J.G. Tests for the characterisation of original Groningen masonry. Delft University of Technology. Final report 18 December 2015.

[2] Jafari S. and Rots, J.G. Summary report for the characterization of original Groningen masonry. Delft University of Technology. Final report 18 December 2015.

[3] Jafari, S. Esposito, R . (2016). Plan of approach for laboratory tests on masonry samples extracted from existing building. Report number C31B67WP1-1, version 06, 20 September 2016.

[4] EN 1996-1-1+A1 (2013). Eurocode 6 – Design of masonry structures – Part 1-1: General rules for reinforced and unreinforced masonry structures. Nederlands Normalisatie-instituit (NEN).

[5] Jafari, S. Esposito, R. (2017). Material characterisation of masonry: Protocol for destructive tests. Delft University of Technology. Report number C31B67WP1-4, version 02, 19 July 2016.

[6] Contractor responsibilities. Technical note by ARUP.

[7] EN 772-1 (2000). Methods of test for masonry units - Part 1: Determination of compressive strength. Nederlands Normalisatie-instituit (NEN).

[8] NEN 6790 (2005). Technical principles for building structures - TGB 1990 - Masonry structures - Basic requirements and calculation methods. Nederlands Normalisatie-instituit (NEN).

[9] EN 1052-1 (1998). Method of test masonry – Part 1: Determination of compressive strength. Nederlands Normalisatie-instituit (NEN).

[10] Van Mier, J.G.M. (1984) Strain Softening of concrete under multiaxial loading conditions, PhD thesis, Eindhoven University of Technology.

[11] Lourenco, P.B., De Borst, R. and Rots, J.G. (1997). A plane stress softening plasticity model for orthotropic materials. International Journal for Numerical Methods in Engineering 40(21), 4033-4057.

[12] EN 1052-2 (1999). Method of test masonry – Part 2: Determination of flexural strength. Nederlands Normalisatie-instituit (NEN).

[13] Pluijm R. Out-of-plane bending of masonry behaviour and strength: Technische Universiteit Eindhoven; 1999.

[14] EN 1052-5 (2005). Method of test masonry – Part 5: Determination of bond strength by bond wrench method. Nederlands Normalisatie-instituit (NEN).

[15] EN 1052-3 (2002). Method of test masonry – Part 3: Determination of initial shear strength. Nederlands Normalisatie-instituit (NEN).

Appendix A – Statues of samples prior to testing

Sample	Picture	Description
TIL-CV-A	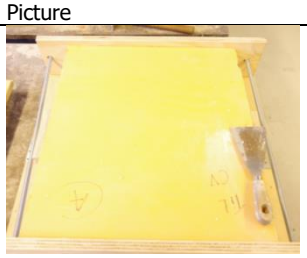 	Specimen arrived in good condition. Sample was covered with plaster. After removal of plaster the sample was subjected to vertical compressive load
TIL-CV-B	 	Specimen arrived in good condition. Sample was covered with plaster. After removal of plaster the sample was subjected to vertical compressive load
TIL-CV-C		Specimen arrived in good condition. Sample was covered with plaster. After removal of plaster the sample was subjected to vertical compressive load
TIL-CH-A		Specimen arrived in good condition. Sample was covered with plaster. After removal of plaster the sample was subjected to horizontal compressive load
TIL-CH-B	 	Specimen arrived in good condition. Sample was covered with plaster. After removal of plaster the sample was subjected to horizontal compressive load

TIL-CH-C			Specimen arrived in good condition. Sample was covered with plaster. After removal of plaster the sample was subjected to horizontal compressive load
TIL-SH1-A	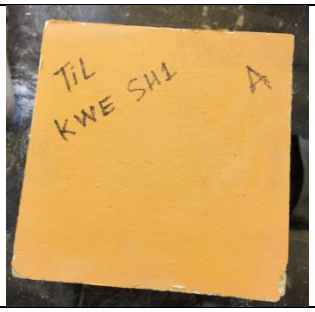		Specimen arrived in good condition. Sample was covered with plaster. Partial disintegration of sample during preparation
TIL-SH1-B			Specimen arrived in good conditions. Sample was covered with plaster. Partial disintegration of sample during preparation.
TIL-SH1-C	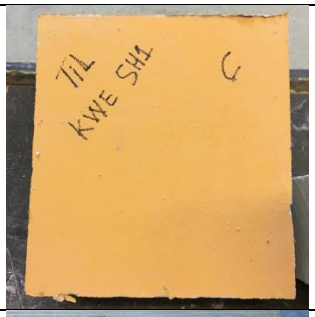		Specimen arrived in good conditions. Sample was covered with plaster.
TIL-SH1-D			Specimen arrived in good condition. Sample was covered with plaster. Full disintegration during plaster removal. No sample to be tested
TIL-SH1-E			Specimen arrived in good condition. Sample was covered with plaster. After removal of plaster was subjected to shear-compression load.

TIL-SH1-F			Sample arrived disintegrated. The disintegration occurred on the bed and head joint of top half brick couple. No sample for testing.
TIL-SH1-G		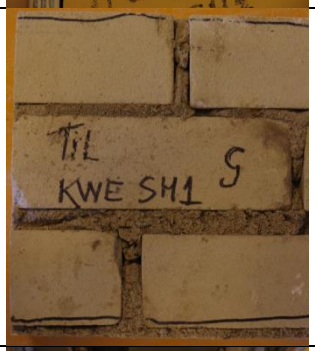	Specimen arrived in good condition. Sample was covered with plaster. After removal the sample was subjected to shear-compression laod.
TIL-SH1-H			Specimen arrived in good conditions. Sample was covered with plaster. Disintegration of sample during plaster removal. Not suitable for the test.
TIL-SH1-I			Specimen arrived in good condition. Sample was covered with plaster. Shear test was performed after removing of plaster.
TIL-SH1-J			Specimen arrived in good condition. Sample was covered with plaster.
TIL-OOP1-A			Specimen arrived in good condition. Vertical out of plane bending test was performed.

TIL-OOP1-B		Specimen arrived in good conditions. Vertical out of plane bending test was performed.
TIL-OOP1-C		Specimen arrived in good conditions. Vertical out of plane bending test was performed.
TIL-OOP2-A		Specimen arrived in good conditions. Horizontal out of plane bending test was performed.
TIL-OOP2-B		Specimen arrived in good conditions. Horizontal out of plane bending test was performed.
TIL-OOP2-C		Specimen arrived in good conditions. Horizontal out of plane bending test was performed.

TIL-IP-A		Specimen arrived in good conditions. In-plane bending test was performed.
TIL-IP-B		Specimen arrived in good conditions. In-plane bending test was performed.
TIL-IP-C		Specimen arrived in good conditions. In-plane bending test was performed.
HOG1-OOP1-A		Specimen arrived in good conditions. During preparation for testing sample was disintegrated. No sample to be tested.
HOG1-OOP2-C		Specimen arrived in good conditions. Horizontal out-of-plane bending test was performed.
TIL-B (12 bricks)		
HOG1-B (12 bricks)	 	Bricks were covered with mortar. The mortar was removed prior to testing.

KWE-B (12 bricks)	
HOOF-B (12 bricks)	Extraction took place but no sample was delivered to the laboratory